NPL
National Physical Laboratory

NPL REPORT MAT 93

REVIEW OF METHODS FOR MODELLING TWO-PHASE PHENOMENA IN A POLYMER ELECTROLYTE MEMBRANE FUEL CELL (PEMFC)

EDMUND J.F. DICKINSON

JULY 2020

REVIEW OF METHODS FOR MODELLING TWO-PHASE PHENOMENA IN A POLYMER ELECTROLYTE MEMBRANE FUEL CELL (PEMFC)

Edmund J.F. Dickinson
Department of Electromagnetic & Electrochemical Technologies

ABSTRACT

This report summarises the development and contemporary state-of-the-art of methods for modelling the role of liquid water (“two-phase phenomena”) in relevant parts of polymer electrolyte membrane fuel cells (PEMFCs). The review focuses on low temperature PEMFCs, considering theoretical methods applicable to the assessment of water transport effects in continuum models, in which water content may be treated as a locally homogenised variable. The review aims to provide a documentary, definitional basis for future comparison between theoretical methods.

ISSN 1754-2979

https://doi.org/10.47120/npl.MAT93

National Physical Laboratory
Hampton Road, Teddington, Middlesex, TW11 0LW

Approved on behalf of NPLML by
Gareth Hinds, Science Area Leader.

CONTENTS

1. INTRODUCTION

This report summarises the development and contemporary state-of-the-art of methods for modelling two-phase flow in relevant parts of polymer electrolyte membrane fuel cells (PEMFCs). By "two-phase flow", we mean models that explicitly describe liquid water as a distinct phase; this is common nomenclature, but is strictly a misnomer since PEMFCs universally contain, as well as gas and liquid water, a distinct ionomer phase in which water transport also occurs.(1)

In this review we focus on low temperature PEMFCs where, unlike for high temperature PEMFCs ("HT-PEM" technology), liquid water condensation cannot be excluded. The review also limits its focus to methods applicable to the assessment of water transport effects in continuum models, in which water content may be treated as a locally homogenised variable. We do not attempt a detailed review either of numerical techniques resolving explicit microstructure or those tracking the phase interface in detail, such as the volume-of-fluid method and lattice Boltzmann method. Equally, we do not discuss the detailed application of more abstract numerical analyses, such as pore network models. Applications to the transient analysis of cold start conditions, which implicate ice as an additional phase for water content, will also be excluded.

For over a decade, two-phase transport models have been identified alongside membrane and catalyst layer models as a key area of PEMFC theory where development is required.(2) Membrane and catalyst layer models were reviewed previously by the present author (1, 3), excluding two-phase phenomena in the latter discussion of the catalyst layer. Two-phase transport phenomena have been reviewed frequently in the PEMFC literature, and historical trends can be assessed by consulting the clearest and most comprehensive reviews, cited hereafter.(4-14)

A natural question to pose in such a review is: what model is best? In more refined form, we may ask: under what circumstances is a particular model appropriate? What conditions of operation would cause a certain model to no longer yield a reasonable prediction of behaviour in the PEMFC? Regrettably, these questions are difficult to answer given the available data. Different models may predict the same experimental data equally well, but it is very unusual to encounter a set of experimental data approached by more than one theoretical route. Moreover, it has been established that different models may reproduce a polarisation curve equally well, while making starkly different predictions with respect to spatially resolved properties (15) such as reactant concentration, temperature, etc., that may be unobservable without *in situ* or *operando* measurement capabilities.

In this review, the goal is to provide a documentary, definitional underpinning whereby the legacy of different approaches can be characterised. This can, in turn, guide future comparison between theoretical methods. The PEMFC modelling literature has yielded an extraordinary variety of extensively parameterised models; regrettably, the often incomplete or ambiguous description of model equations in published works increases the challenge of identifying unifying trends, but it is certainly possible to identify a number of significant advances in understanding and 'best practice', as well as the central questions that remain open for future study.

1.1. WHY IS LIQUID WATER RELEVANT?

The essential challenge of water management in a PEMFC is that the membrane must remain hydrated in order to maintain its proton conductivity, but water supersaturation leads to condensation ("electrode flooding") that may limit current density by blocking transport of reactant gases to reaction sites in the catalyst layer (CL) and/or by blocking diffusion of reactant gases in the gas diffusion layer (GDL).(16) Additionally, electro-osmotic drag in the membrane draws water from anode to cathode alongside the current-carrying protons. "Back-diffusion" of water in the cathode-to-anode direction through the membrane is required to maintain adequate membrane hydration on the anode face; otherwise, anode humidification must be maintained in order to support overall water balance. Since

anode humidification eliminates the driving force for back-diffusion, it has been described as "self-defeating" from the perspective of overall water management.(17)

As with models of the catalyst layer and electrode kinetics, significantly more focus has been placed in the literature on two-phase transport models for the cathode than the anode, due to the much greater contribution of the cathode to transport-controlled losses in operation. When the cathode inlet is at 100% relative humidity (RH), at least some liquid water is expected on the cathode side (18), due to the net water source from the cathode half-cell reaction (oxygen reduction reaction, ORR):

$$O_2 + 4H^+ + 4e^- \rightarrow 2H_2O \qquad [1.1]$$

Typically, flooding in the cathode CL will precede flooding in other regions, since this is the origin of the net water source, and the CL is comparatively hydrophilic with relatively low porosity and small pores.(19) For operating conditions of 500 mA cm^{-2}, the water source at a PEMFC cathode is 46.6 μg cm^{-2} s^{-1} ≈ 48 nL cm^{-2} s^{-1} as liquid, at the typical operating temperature of conventional low temperature PEMFCs (T = 80 °C). The vapour-phase water storage capacity of the gas-phase at 100% relative humidity at the same temperature is ≈ 13 μg cm^{-3}. Water content retention then arises through the balance of the water generation rate, storage capacity, evaporation rate and both vapour- and liquid-phase water transport.(20) Equilibration timescales for water transport are typically in the range of seconds to minutes, and are typically much slower than the corresponding equilibration timescales for proton transport.(21)

The ratio of water production to maximal rate of water removal by the vapour diffusion pathway (Damköhler number) has been characterised as a key dimensionless variable for different regimes of GDL water transport (all variable notation is summarised in the Table of Symbols in the Appendix):(22)

$$\mathrm{Da} = \frac{i_{\mathrm{cell}} RT}{2F} \frac{d_{\mathrm{GDL}}}{D_{\mathrm{eff,w}} p_{\mathrm{vap}}} \qquad [1.2]$$

For Da ≈ 1, partial but not saturated liquid water content is expected.

1.2. DIMENSIONAL ANALYSIS

Water transport in PEMFC porous media (that is, the GDL and CL as well as a possible microporous layer (MPL) dividing them) occurs in pores with diameters no larger than 50 μm.(23) Gas and water velocities at a typical operating current density (1 A cm^{-2}) and with typical operating pressure (> 1 bar) evaluate to < 1 mm s^{-1}. Accordingly, the flow is absolutely laminar within PEMFC porous media, tending towards the Stokes flow regime (Reynolds number < 0.01). Using the water-air surface tension (60-65 mN m^{-1} at fuel cell operating temperature) yields a capillary number for liquid water < 10^{-7}; equally, considering water droplets of radius of order 1 μm suggests an Eötvös number ≈ 10^{-7}, while even for water droplets with radius matching the largest pore diameters, Eo < 10^{-3} (some authors have reported much lower values but these do not seem to be supported by computation from material properties). These two results make plain that both inertial and gravitational forces are completely dominated by surface tensile forces for typical GDL conditions.(14, 24-27) Therefore, gravity is almost always neglected in two-phase models for PEMFC porous media, and turbulence-free drag approximations such as Darcy's law (discussed further below under "Two-phase Darcy's law") are appropriate for the fluid dynamics.

1.3. CONSERVATION RELATIONS

Liquid water content in porous media is conventionally characterised according to its saturation s_l, which is the volume fraction of the void space occupied by liquid water. Consequently, for region i of the PEMFC (e.g. GDL, MPL, CL) with dry porosity $\varepsilon_{i,\mathrm{dry}}$, the volume fraction of liquid water (with respect to unit composite volume) is given:

$$\varepsilon_l = s_l \varepsilon_{i,\mathrm{dry}} \qquad [1.3]$$

The volume fraction of the gas phase is:

$$\varepsilon_{\mathrm{g}} = (1 - s_{\mathrm{l}})\,\varepsilon_{i,\mathrm{dry}} \qquad [1.4]$$

A general conservation equation for liquid water can be written:(28-30)

$$\frac{\partial\left(\rho_{\mathrm{w}}\varepsilon_{i,\mathrm{dry}}s_{\mathrm{l}}\right)}{\partial t} + \nabla\cdot\mathbf{N}_{l} = R_{\mathrm{w}} \qquad [1.5]$$

1.4. GAS DIFFUSION LAYER PROPERTIES

The specific materials used for the GDL (or "diffusion media") have a major impact on its water transport properties. Conventionally, the GDL is made of conducting carbon (fibre or cloth) impregnated with a hydrophobic additive (such as polytetrafluoroethylene, PTFE) whose purpose is to prevent flooding by promoting "wicking" of water out of the GDL.(31) The presence of hydrophobic additives creates a mixed wettability material, complicating the analysis of capillary action in the GDL.

Hydrophobic additives must be incorporated to an optimal extent, since excessive GDL hydrophobicity may cause excess water retention in the ionomer content of the adjacent catalyst layer, leading to flooding. Material optimisation is also condition-dependent, generally speaking: for instance, carbon cloth has been reported to perform well in wet conditions due to superior water removal, whereas carbon paper performs well in dry conditions due to superior water retention.(32) Zamel et al. provided a detailed review of measurement data to 2013, considering also data utilisation in the form of effective media properties.(10)

1.5. ROLE OF A MICROPOROUS LAYER

It is known that performance can be improved by including a hydrophobic microporous layer (MPL), of lower porosity and permeability than the GDL, between the CL and GDL. Specifically, MPL pore size is characteristically < 1 μm, while normal GDL materials have pore sizes > 10 μm.(32, 33) The role of water transfer in the mechanism of MPL performance enhancement remains a subject of debate, but there is a general consensus that its importance lies in promoting water retention in the CL and membrane without increasing water saturation in the GDL; in effect, a barrier or buffer layer between the CL and GDL is generated.(34) Some authors have argued that the MPL directly promotes water retention in the cathode CL and back-diffusion to the anode.(35) Other authors see the MPL as encouraging distinct thermal environments between GDL and CL by creating distinct evaporation-condensation regimes or acting as a barrier to material transport (36); the MPL may also simply reduce interfacial contact resistance (37) or improve transport into the CL by providing it with mechanical support and eliminating volume intrusion of the CL into the larger GDL pores (38). Condensation of water vapour leaving the MPL on entering the more hydrophilic GDL has been noted experimentally.(34)

1.6. ROLE OF HEAT TRANSFER

Liquid water transport interacts universally with the transfer of heat in operating PEMFCs, especially since temperature gradients imply relative humidity gradients.(34, 36) A discussion on heat transfer in PEMFCs will be the subject of a separate review. It is important to recognise that in practical scenarios, the intrinsic temperature-dependence of driving forces and rates for evaporation and condensation mean that two-phase transport phenomena cannot be decoupled from heat transfer phenomena occurring in the fuel cell.(36)

Neutron imaging results demonstrate a qualitative change in behaviour at $T \geq 80$ °C, with an evaporation-driven heat pipe effect ("phase change-induced flow") beginning to dominate droplet emergence as the chief mechanism for exhaust of liquid water from the GDL to the gas channels.(34, 39, 40) In other circumstances, differences in evaporation rate on the two faces of the membrane may

induce water flow through the membrane.(41) Another significant non-isothermal effect is the role of thermal resistance; electrodes that displace heat less effectively – for example, due to the presence of a microporous layer (MPL), as noted above – will reach a higher temperature with respect to the inlet gas, and so will also tend to evaporate water more readily.(23)

1.7. OVERALL PERSPECTIVE

As for other features of PEMFC modelling, the literature contains a superfluity of detailed studies with minimal mutual variation and frequent dependence upon thinly justified approximations, such as the ubiquitous "Leverett function" (see "Relation of capillary pressure to saturation", below). An accompanying literature review spreadsheet is available on request to document the combination of methods used in prior works.

Increased computational power in the last twenty years has encouraged progressively more detailed models to be created, and has led to some changes in 'fashion' in two-phase flow modelling. Simultaneously, progress on understanding of the dynamics of liquid water has arisen from *in situ* experimental observations on transparent fuel cells (42-44) and neutron imaging experiments (34, 45). In some cases, limitations in present methodologies have been remarked upon without any theoretical methods being developed to address them – for example, cracks in the MPL and CL may have a significant impact on water transport behaviour, but are most often ignored by water transport models. (16, 46)

This report is structured into three principal themes. Sections 2-6 formulate the various standard systems of equations used in literature to describe homogenised two-phase phenomena. Sections 7-8 address the parameterisation of these systems of equations in GDL materials, variously from fundamental considerations, empirical experimentation on PEMFC porous media (typically *ex situ*), or analogies to the literature on porous media in other fields of applied science. Sections 9-11 address the incorporation of two-phase phenomena in models of the MPL, gas channel and catalyst layer regions of a PEMFC, respectively.

2. PSEUDO-TWO-PHASE TREATMENTS

A number of simple "pseudo-two-phase" models have been developed to account for some effects of the liquid water phase, without implementing a two-phase flow model. Due to the reduction in computational cost associated with avoiding a more rigorous two-phase flow model, these approaches have been especially popular for models on detailed 3D structures, including flow channels (47-49), and/or under transient conditions (50, 51).

2.1. WATER BALANCE COMPUTATION ONLY

Early works by Bernardi et al. (52) and Fuller et al. (53) computed water balance, but did not consider evaluate any consequences of the evaluated liquid water content as an influence feeding back on cell performance. Springer et al. (54) treated the liquid water as a blocking species that occupies volume and so reduces porosity (in effect considering it as a solid (55)), but as having no other impact on performance. The Springer "blocking water" model has subsequently been combined with a water transport model based on a constant capillary diffusion coefficient.(56)

Other models have considered liquid water transport to occur in parallel with gas transport, in the presence of an evaporation-condensation equilibrium between the two phases.(57-59) This type of model is inspired by the concept of separate but parallel flow paths in PTFE-impregnated (hydrophobic) and PTFE-free (hydrophilic) channels (57), and implicitly considers water transport to be driven by inertia under the saturation gradient, without any capillary action contributing to the transport, or any influence of liquid water saturation on CL reaction rate or reactant transport. A comparable model has been proposed to describe the CL at low humidity, considering water transport in gas and membrane phases subject to a sorption equilibrium, while excluding the liquid phase.(60) A

similar approach, assuming additionally that condensed water reduces reaction current densities proportionally to saturation, has also been applied to analyse the role of pore size distribution in the GDL, and in flow channel design.(61, 62)

2.2. EMPIRICALLY DEFINED WATER VOLUME FRACTION

Another simple approach is to define a series transport resistance, where oxygen transport occurs more slowly within a defined proportion f_w of the 1D transport path through the GDL that is assumed occupied by liquid water.(63, 64) Similarly, the water volume fraction in the partially flooded CL can be interpreted as a water film, and an additional resistance can be included within the electrode kinetic expression.(65) Wherever this model has been applied, the water volume fractions are considered global properties of the GDL under a given set of operating conditions, and are defined empirically through fitting to experiment, rather than being solved self-consistently from a two-phase transport model.

2.3. LIQUID WATER AS A DIFFUSING SPECIES ("WET GAS" MODEL)

"Pseudo-two-phase" models are most often developed by neglecting momentum transfer between the liquid and gas phases, and so treating liquid water as an additional diffusing species within a single-phase flow, as though the liquid is present as infinitesimal droplets in a "wet gas".(49, 66-70) This simplification of the momentum balance and diffusional/capillary transport allows the mass and energy balance for liquid water generation and removal to be evaluated self-consistently; although most of the above-cited models are vague about how the density of the "wet gas" phase is computed, in general it is implied that the liquid water component is treated as having the density of liquid water and contributes to the overall phase density proportionally to its composition (69).

The "wet gas" approach has been extended by using the local "liquid water" mass concentration in the catalyst layer to define a water film thickness, allowing an additional transport resistance for oxygen transport to be quantified, but without introducing any further correction to the permeability or tortuosity of the porous material, or a more refined description of the influence of liquid water on the catalytic turnover rate in the kinetic equations.(51, 71) The "wet gas" model has also been combined with a saturation-dependent effective permeability for the porous media.(72)

2.4. PSEUDO-EQUILIBRIUM

For cases where both water vapour and liquid water are assumed to be present throughout the channel, the assumption that equilibrium between the phases is maintained locally by the evaporation-condensation process allows the water saturation level to be determined directly.(73, 74) For instance, effective fluid properties for a single-phase flow model may be defined as a linear combination of the gas- and liquid-phase fluid properties.(73) Alternatively, a model has been proposed solving only for the gas-phase species, but making this gas-phase diffusion model saturation-dependent by expressing liquid water saturation as the excess mass of water vapour above the relative humidity.(75)

3. THEORIES BASED ON NON-EQUILIBRIUM THERMODYNAMICS

Fundamental non-equilibrium thermodynamics provides a basis for general theories of multiphase transport, subject to empirical determination of transport coefficients.(76, 77) The most general theories have tended to be largely disfavoured compared to theories with less phenomenological parameterisation, such as the two-fluid model to be discussed below.

Janssen made an attempt towards a consistent, phenomenological model based on a generic chemical potential for liquid water, with effective drag coefficients to express the relation of gas-phase to liquid-phase transport.(78) As a principally empirical theory based on non-equilibrium thermodynamics, the Janssen liquid water theory matches naturally with the approach of the Weber-Newman membrane model (1, 79), which also uses a generic chemical potential for membrane-phase water and defines fluxes from non-equilibrium thermodynamics. Janssen's work assumes that liquid- and vapour-phase

water transport occurs in parallel through separate pores, with no mutual equilibration except at the membrane interface; also, it is restricted to isothermal conditions with constant gas-phase pressure and Maxwell-Stefan diffusion in the GDLs. Further, it appears that Janssen's work, like the earliest work by Weber and Newman (80), does not consider the influence of liquid water saturation on the gas-phase volume fraction and tortuosity; this was corrected in later work from the Newman group (6). Janssen has pointed out that Maxwell-Stefan diffusion requires non-uniformity in the partial pressure of water vapour through the GDL, due to the flux of H_2 or O_2 gas.(78)

4. TWO-PHASE DARCY'S LAW

4.1 RICHARDS' EQUATION AND TWO-FLUID MODEL

The most widely adopted description for two-phase flow in PEMFC porous media is based on Darcy's law, which is the approximation that, at low Reynolds number (see Section 1.2, "Dimensional analysis", above), there is a linear relationship between effective velocity and pressure gradient:(77)

$$\mathbf{N}_k = -\rho_k \frac{\kappa_k}{\mu_k} \nabla p_k \qquad [4.1]$$

where phase k has density, ρ_k, dynamic viscosity μ_k, and absolute pressure p_k. The permeability κ_k (units of area, m^2) is an empirical measure of the drag force exerted by the solid structure of the porous medium.

The effective velocity measured per unit cross-sectional area of the composite porous material is then given as the ratio of total mass flux to density, and is defined as the Darcy velocity $\mathbf{u}_k$:

$$\begin{aligned} \mathbf{u}_k &\equiv \frac{\mathbf{N}_k}{\rho_k} \\ &= -\frac{\kappa_k}{\mu_k} \nabla p_k \end{aligned} \qquad [4.2]$$

Two-phase Darcy's law assumes that, for two-phase flow in porous media, Darcy's law applies independently to both the liquid and gas phases. The permeabilities are then functions of the saturation, since the two phases occupy separate volume fractions within the pore space and therefore gas flow occurs in a restricted network of gas channels between the liquid water regions, and *vice versa*. As a homogenised model of the composite porous material, two-phase Darcy's law makes no specific assumptions regarding the topology or morphology of the liquid and gas phases; morphological effects are expressed only through the value of the permeability κ_k.

$$\mathbf{u}_\mathrm{g} = -\frac{\kappa_\mathrm{g}}{\mu_\mathrm{g}} \nabla p_\mathrm{g} \qquad [4.3]$$

$$\mathbf{u}_\mathrm{l} = -\frac{\kappa_\mathrm{l}}{\mu_\mathrm{l}} \nabla p_\mathrm{l} \qquad [4.4]$$

In the classical unsaturated flow theory of groundwater transport in rocks and soils, a local capillary pressure p_cap is defined as the averaged local difference between the non-wetting and wetting phase pressures.(81-83) In hydrophilic media, where the liquid phase (water) is the wetting phase:

$$p_\mathrm{cap} = p_\mathrm{g} - p_\mathrm{l} \qquad [4.5]$$

It is crucial to note that the majority of PEMFC literature retains the definition of the quantity notated p_cap from [4.5] even in hydrophobic media, where liquid water becomes the non-wetting phase. In the latter case, the capillary pressure itself (a strictly positive quantity) becomes the negative of the quantity denoted p_cap. For consistency with published literature, we will retain the notational definition from [4.5] throughout and refer to it as "capillary pressure", while recognising that this disagrees with the conventional meaning of the term in the physics of phase interfaces.

According to the energetics of the two-phase interface and the interactions of both phases with the wetted solid, the local capillary pressure is expected to depend on the topology of the two-phase interface. In the simple case of a spherical meniscus, the Young-Laplace equation relates capillary pressure to the radius of curvature of the two-phase interface (see further discussion below in Section 7.6, "Pore-size distribution analysis: capillary pressure and saturation"). For partially saturated composite media, the particular geometry of the two-phase interface will be complex and difficult to predict; however, it is commonly treated as an empirical function of the local degree of liquid water saturation, since as the liquid water content of the pores increases, the morphology will evolve and the characteristic radii of curvature of the liquid-gas interface will change. In this way, the capillary pressure is then approximated as an empirical function of liquid water saturation, with the functional dependence being material-specific (see further discussion below in Section 7.2, "Relation of capillary pressure to saturation"). Through its dependence on surface tension, the capillary pressure may also depend on temperature, as well as the concentrations of any solutes in the liquid water (Gibbs-Marangoni effect).

Given the much lower density of the gas phase compared to the liquid phase, it is common to assume that the gas-phase pressure remains approximately constant under slow flow conditions. Then, if p_g is constant:

$$\nabla p_{\text{cap}} \approx -\nabla p_{\text{l}} \tag{4.6}$$

Therefore:

$$\mathbf{u}_{\text{l}} = \frac{\kappa_{\text{l}}}{\mu_{\text{l}}} \nabla p_{\text{cap}} \tag{4.7}$$

Combined with the conservation relation [1.5] and the relation of effective mass flux to Darcy velocity given by [4.2], assuming the liquid is pure water:

$$\frac{\partial \left(\rho_{\text{w}} \varepsilon_i s_{\text{l}} \right)}{\partial t} = -\nabla \cdot \left(\frac{\rho_{\text{w}}}{\mu_{\text{w}}} \kappa_{\text{l}} \nabla p_{\text{cap}} \right) + R_{\text{w}} \tag{4.8}$$

Under the approximation that water density is constant and that p_{cap} can be expressed as a function of the liquid water saturation s_{l} alone (that is, assuming negligible temperature gradients and ignoring any solutes):

$$\frac{\partial \left(\varepsilon_i s_{\text{l}} \right)}{\partial t} = -\nabla \cdot \left(\frac{\kappa_{\text{l}}}{\mu_{\text{w}}} \frac{\partial p_{\text{cap}}}{\partial s_{\text{l}}} \nabla s_{\text{l}} \right) + \frac{R_{\text{w}}}{\rho_{\text{w}}} \tag{4.9}$$

This is *Richards' equation*. It is possible to interpret this equation as a (nonlinear) diffusion equation in the liquid-phase saturation, where the corresponding capillary diffusion coefficient is:

$$D_{\text{cap}} = -\frac{\kappa_{\text{l}}}{\mu_{\text{w}}} \frac{\partial p_{\text{cap}}}{\partial s_{\text{l}}} \tag{4.10}$$

such that

$$\frac{\partial \left(\varepsilon_i s_{\text{l}} \right)}{\partial t} = \nabla \cdot \left(D_{\text{cap}} \nabla s_{\text{l}} \right) + \frac{R_{\text{w}}}{\rho_{\text{w}}} \tag{4.11}$$

For hydrophobic media, the capillary diffusion coefficient is negative and the prevailing driving force of capillary action is to transport water *up* a saturation gradient, as discussed further below under Section 7.3, "Capillary diffusion coefficient", below.

For the case where the gas-phase pressure may vary appreciably, and so [4.6] does not hold, a more general treatment is needed. In this case, the assumption of independent Darcy's laws for each phase allows us to write:

$$\begin{aligned} -\nabla p_{\mathrm{l}} &= -\nabla p_{\mathrm{g}} + \nabla p_{\mathrm{cap}} \\ &= \frac{\mu_{\mathrm{g}} \mathbf{u}_{\mathrm{g}}}{\kappa_{\mathrm{g}}} + \nabla p_{\mathrm{cap}} \end{aligned} \qquad [4.12]$$

Hence:

$$\begin{aligned} \mathbf{u}_{\mathrm{l}} &= \frac{\kappa_{\mathrm{l}}}{\mu_{\mathrm{l}}} \left(\frac{\mu_{\mathrm{g}} \mathbf{u}_{\mathrm{g}}}{\kappa_{\mathrm{g}}} + \nabla p_{\mathrm{cap}} \right) \\ &= f_{\mathrm{s}} \mathbf{u}_{\mathrm{g}} - D_{\mathrm{cap}} \nabla s_{\mathrm{l}} \end{aligned} \qquad [4.13]$$

The quantity f_{s} represents a shear interaction between the liquid-phase and gas-phase flows, as quantified by the permeabilities and pressure fields for each phase:

$$f_{\mathrm{s}} = \frac{\kappa_{\mathrm{l}}}{\kappa_{\mathrm{g}}} \frac{\mu_{\mathrm{g}}}{\mu_{\mathrm{l}}} \qquad [4.14]$$

[4.13] can be solved alongside [4.3] within the conservation relation [1.5] to give a liquid water conservation equation, which subject to the approximation of constant water density reads:

$$\frac{\partial \left(\varepsilon_i s_{\mathrm{l}} \right)}{\partial t} = \nabla \cdot \left(D_{\mathrm{cap}} \nabla s_{\mathrm{l}} - f_{\mathrm{s}} \mathbf{u}_{\mathrm{g}} \right) + \frac{R_{\mathrm{w}}}{\rho_{\mathrm{w}}} \qquad [4.15]$$

The theory described by equation [4.15], in which liquid-phase mass transport is expressed as a combination of shear drag and capillary diffusion, is usually referred to as the *two-fluid model* (84). This theory has historically been the most popular approach for two-phase PEMFC models, especially within the last decade.

An important issue relating to the use of Richards' equation or the two-fluid model is the risk of a singularity at $s_{\mathrm{l}} = 0$. The existence of a discontinuity between the case of zero saturation and finite but negligible saturation is an example of a front-tracking problem, where a moving phase front divides regions where liquid water is either present or completely absent.(85, 86) A number of distinct cases with sharp interfaces between dry and partially saturated porous media have been explored (87-89). All numerical approaches to the front-tracking problem relate closely to the treatment of the evaporation-condensation reactions.(86)

It has been suggested that the application of [4.15] asserts saturation continuity at interfaces between different porous media (for example, the MPL-GDL interface) (90); no such constraint is inherent in the derivation, however. Rather, it is generally recognised that there exists physical requirement of continuous *pressure* of each phase at the material boundaries between different regions (for example, gas-phase pressure is continuous across the GDL-MPL interface, as is liquid-phase pressure).(91) This pressure continuity implies a saturation discontinuity; therefore, saturation should not be considered a uniformly smooth dependent variable in two-fluid models.(92)

4.2 APPLICATION OF TWO-FLUID MODELS TO PEMFC SIMULATION

In a highly influential 2000 work, He et al. presented the first application of a two-phase Darcy's law to describe two-phase flow in the cathode GDL, according to the two-fluid model [4.15] and including a specified condensation-evaporation rate (see "Evaporation-condensation"). This work used constant values of $f_{\mathrm{s}} = 0.005$ and $D_{\mathrm{cap}} = 10^{-8}$ m^2 s^{-1}, on the basis that the range of saturations considered was narrow. In this work, the boundary condition for gas-phase velocity at the GDL-CL interface set a value of zero, which incorrectly neglects the Stefan velocity due to O_2 consumption.

Natarajan et al. continued this work up to a 2D+1D control volume model for a 3D GDL, including the Richards' equation approximation that the gas-phase velocity can be completely neglected. In this case, capillary action is the only mechanism of liquid-phase transport.(28, 93) The Richards' equation

(capillary action-only) model has subsequently been followed by a number of other authors (94), including in combination with a physically detailed saturation-dependent membrane model (6, 95). Two-phase Darcy's law has also been combined with a "general transport equation" (96, 97), although this result appears to be essentially equivalent to an empirically parameterised non-equilibrium thermodynamics approach, and does not facilitate material property determination.

A full summary of PEMFC models using a two-phase Darcy's law is given in the accompanying spreadsheet. The works of Song et al. (98) and Akhtar et al. (99) may be considered to be particularly 'standard' implementations, using the most common parameterisations of capillary pressure, liquid-phase permeability, and evaporation-condensation rate (see also "Thermodynamic properties and constitutive relations for partially saturated porous media" below). Some relevant extensions include: the addition of a magnetic force term to account for magnetic particles (100); non-isothermal flow (101); transient analysis (102) with particular focus on hysteresis (103); local thermal non-equilibrium (104); thermal anisotropy (105); cold start conditions (106); inlet transients for gas humidification (107); compression-dependent tortuosity and permeability of the porous media (108); electrodes with low Pt loading (109); incorporation of anode CO contamination (110); and non-uniform catalyst layers (111, 112). The results of a 3D non-isothermal two-fluid model were recently compared to spatially resolved water content measurements from neutron radiography data, with good agreement on the distribution of liquid water through a serpentine flow field.(113)

4.3 CRITICISM OF TWO-FLUID MODELS

Two-phase Darcy's law has a substantial legacy of success in the modelling of partially saturated flows in earth sciences (83); however, the prevailing conditions of PEMFC porous media differ in many respects from soils and porous rocks. It is implausible that Darcy's law would hold accurately for both gas and liquid phases independently in the limits where $s_l \rightarrow 0$ or $s_l \rightarrow 1$, such that either the liquid or gas phase respectively ceases to form a connected network. The validity of a steady-state Darcy's law in the PEMFC context has further been queried under transient loading (87) and criticised as inappropriate for high reaction rate conditions (24). In particular, the consumption of gaseous reactant mass in PEMFCs means that gas pressure gradients may be more significant than implied by the flow regimes alone, and the Richards' equation approximation of constant gas phase pressure is unlikely to be valid.(114)

More controversially, Gurau et al. also assert that mass exchange between phases should introduce a momentum source term in the two-fluid model or any of its simplifications.(92) This is a fundamental question in the theory of homogenised descriptions of multiphase porous media, to which no unambiguous solution has yet been provided in the literature. The response of Wang et al. is that the missing momentum balance corresponds to the Darcy's law assumption in which inertia is neglected ($Re \rightarrow 0$), such that the drag exerted by the solid porous matrix on the fluids is always sufficient to instantaneously damp any 'excess' momentum(115); this is a persuasive argument. A rigorous re-analysis of the mass and momentum balance equations, returning to the fundamental literature (116), could be valuable to resolve these concerns.

Comparison to chronoamperometric measurements has suggested that two-phase flow models based on two-phase Darcy's law should be interpreted qualitatively, and that the reliability of these methods for appreciably hydrophobic materials can be poor.(84) Analysis of SEM data in the latter work suggested that GDL materials with more hydrophobic composition can exhibit stochastic behaviour in the formation of liquid films and droplets, undermining the continuum approach and favouring the exploration of resolved interface and lattice Boltzmann methods.

5. MULTIPHASE MIXTURE (M^2) MODEL

5.1 DEFINITION OF THE M^2 MODEL

The multiphase mixture (M^2) model is the chief competitor to the two-fluid model in numerical descriptions of two-phase flow in PEMFCs, although it shares many of the same approximations. The

initial formulation of this theory (117, 118) and its application to PEMFCs (119) was by Wang et al.; a more modern, practical summary has been given by Pasaogullari and Wang (120).

The M^2 model shares the assumptions of the two-fluid model:

- Two-phase Darcy's law holds for momentum transfer in both phases
- A local capillary pressure-saturation relation is maintained.

The M^2 model averages the transport equations over both phases to derive a model for transport for a single "fluid" with highly nonlinear transport coefficients, representing the phase equilibrium and capillary driving force. Like the two-fluid model, if the gas pressure is deemed constant then the M^2 model reduces to Richards' equation.(118) The dry porosity is typically assumed to be constant; that is, the solid matrix in the porous media is non-deformable.

Most often, the M^2 model is used in conjunction with local thermodynamic equilibrium for partition between phases, so that condensation and evaporation of water proceeds at a transport-controlled rate. In this case, the combined transport of a component (such as water) across both phases can be expressed as a single equation. Under the additional equilibrium assumption, the M^2 theory becomes more restrictive than the two-fluid model, but when the approximation of an evaporation-condensation equilibrium is physically acceptable, M^2 theory has been advocated as more computationally efficient (9). It also avoids any need to resolve a sharp interface between unsaturated and partially saturated regions of the fuel cell porous media.

The averaged mass and momentum transport equations are given as follows for the binary liquid-gas system:(117, 119)

$$\varepsilon \frac{\partial \rho}{\partial t} + \nabla \cdot \left(\rho \mathbf{u} \right) = 0 \qquad [5.1]$$

$$\rho = \rho_{\mathrm{l}} s_{\mathrm{l}} + \rho_{\mathrm{g}} \left(1 - s_{\mathrm{l}} \right) \qquad [5.2]$$

$$\frac{1}{\varepsilon}\left(\frac{\partial \left(\rho \mathbf{u} \right)}{\partial t} + \nabla \cdot \left(\rho \mathbf{u}\mathbf{u} \right) \right) = \nabla \cdot \left(\mu \nabla \mathbf{u} \right) - \nabla p + \gamma_{\rho} \rho \mathbf{g} - \frac{\mu}{\kappa_0} \mathbf{u} \qquad [5.3]$$

$$\mu = \frac{\kappa_0 \rho}{\left(\frac{\kappa_{\mathrm{l}} \rho_{\mathrm{l}}}{\mu_{\mathrm{l}}} + \frac{\kappa_{\mathrm{g}} \rho_{\mathrm{g}}}{\mu_{\mathrm{g}}} \right)} \qquad [5.4]$$

$$\gamma_{\rho} = \frac{\lambda_{\mathrm{l}} \rho_{\mathrm{l}} + \left(1 - \lambda_{\mathrm{l}} \right) \rho_{\mathrm{g}}}{\rho} \qquad [5.5]$$

$$\lambda_{\mathrm{l}} = \frac{\left(\frac{\kappa_{\mathrm{l}} \rho_{\mathrm{l}}}{\mu_{\mathrm{l}}} \right)}{\left(\frac{\kappa_0 \rho}{\mu} \right)} \qquad [5.6]$$

$$\begin{aligned} p &= \lambda_{\mathrm{l}} p_{\mathrm{l}} + \lambda_{\mathrm{g}} p_{\mathrm{g}} \\ &= p_{\mathrm{l}} + \lambda_{\mathrm{g}} p_{\mathrm{cap}} \end{aligned} \qquad [5.7]$$

The momentum balance is given by [5.3] in a general (Darcy-Brinkman) form, as applied also to the open gas channels in some works (discussed further below under Section 10.4, "Effective media approximations of the gas channel"). If Darcy's law may be considered applicable due to the small pore size (neglecting inertial effects), as would be typical for PEMFC porous media, [5.3] can be eliminated by expressing the averaged Darcy's law as:(117)

$$\mathbf{u} = -\frac{\kappa_0}{\mu}\nabla p \qquad [5.8]$$

For a binary liquid-gas system containing *n* component species, indexed *i*, the averaged transport equations for the individual species are given as follows:(117)

$$\varepsilon\frac{\partial(\rho w_i)}{\partial t} + \nabla\cdot(\gamma_i \rho w_i \mathbf{u}) = \varepsilon\nabla\cdot\left(\rho_\mathrm{l} s_\mathrm{l} D_{i,\mathrm{l}}\nabla w_{i,\mathrm{l}} + \rho_\mathrm{g}(1-s_\mathrm{l})D_{i,\mathrm{g}}\nabla w_{i,\mathrm{g}}\right) - \nabla\cdot\left(\left(w_{i,\mathrm{l}} - w_{i,\mathrm{g}}\right)\mathbf{j}_\mathrm{l}\right) \qquad [5.9]$$

$$\rho w_i = \rho_\mathrm{l} s_\mathrm{l} w_{i,\mathrm{l}} + \rho_\mathrm{g}(1-s_\mathrm{l})w_{i,\mathrm{g}} \qquad [5.10]$$

$$\gamma_i = \frac{\lambda_\mathrm{l} w_{i,\mathrm{l}} + (1-\lambda_\mathrm{l})w_{i,\mathrm{g}}}{w_i} \qquad [5.11]$$

$$\mathbf{j}_\mathrm{l} = \frac{\kappa_0\rho}{\mu}\lambda_\mathrm{l}\left((1-\lambda_\mathrm{l})\nabla p_\mathrm{cap} - (\rho_\mathrm{l} - \gamma_\rho\rho)\mathbf{g}\right) \qquad [5.12]$$

Of the *n* equations [5.9], only (*n*-1) are independent; correspondingly, only (*n*-1) of the mass fractions w_i are independent (and likewise for $w_{i,\mathrm{l}}$ and $w_{i,\mathrm{g}}$), since the mass fractions must sum to unity across all species. Pasaogullari and Wang have presented a reformulation of these equations in terms of molar concentration rather than mass fraction, which may be more convenient in some circumstances.(120)

To proceed beyond [5.12], the model considers the capillary pressure to be a more general function $p_\mathrm{cap}(s_\mathrm{l},\gamma)$ of saturation and local surface tension γ, in which the local surface tension can in turn be a function of material composition and temperature (Gibbs-Marangoni effect):

$$p_\mathrm{cap} = p_\mathrm{cap}(s_\mathrm{l},\gamma) \qquad [5.13]$$

Thus the diffusive flux of the liquid phase is represented as:

$$\mathbf{j}_\mathrm{l} = \rho_\mathrm{l}\left(-D_\mathrm{cap}\nabla s_\mathrm{l} - \sum_i D_{\mathrm{sol},i}\nabla w_i - D_T\nabla T\right) + \frac{\kappa_0\rho}{\mu}\lambda_\mathrm{l}(\rho_\mathrm{l} - \gamma_\rho\rho)\mathbf{g} \qquad [5.14]$$

$$D_\mathrm{cap} = -\frac{\rho}{\rho_\mathrm{l}}\frac{\kappa}{\mu}\lambda_\mathrm{l}(1-\lambda_\mathrm{l})\left(\frac{\partial p_\mathrm{cap}}{\partial s_\mathrm{l}}\right) \qquad [5.15]$$

$$D_{\mathrm{sol},i} = -\frac{\rho}{\rho_\mathrm{l}}\frac{\kappa}{\mu}\lambda_\mathrm{l}(1-\lambda_\mathrm{l})\left(\frac{\partial p_\mathrm{cap}}{\partial\gamma}\frac{\partial\gamma}{\partial w_i}\right) \qquad [5.16]$$

$$D_T = -\frac{\rho}{\rho_\mathrm{l}}\frac{\kappa}{\mu}\lambda_\mathrm{l}(1-\lambda_\mathrm{l})\left(\frac{\partial p_\mathrm{cap}}{\partial\gamma}\frac{\partial\gamma}{\partial T}\right) \qquad [5.17]$$

The diffusion coefficients parameterise diffusion fluxes that represent relative motion of one *phase* with respect to the mass-averaged motion of both phases. In general, the permeability is a second-order tensor quantity, but most often it is assumed that the permeability is isotropic and so it is represented as a scalar. In the case of heterogeneous permeability, an additional driving force proportional to the gradient of permeability ($\nabla\kappa_0$) is expected.

Altogether, the transport equations of the M^2 model presented from [5.1]-[5.17] comprise *n*+3 independent equations for the *n*-component system and their associated definitions. These independent equations are the overall mass and (three-dimensional) momentum balance equations [5.1] and [5.3], and a set of *n*-1 additional mass balance equations [5.9] for the component species. The unknowns of the problem are the phase-averaged pressure *p*, (three-dimensional) mixture velocity **u**, saturation s_l, and 2(*n*-1) independent component mass fractions $w_{i,\mathrm{g}}$ and $w_{i,\mathrm{l}}$.

Since the number of unknowns ($2n$+3) exceeds the number of equations (n+3), the M^2 model is not closed subject to the statements given so far. In order that $w_{i,\mathrm{g}}$ and $w_{i,\mathrm{l}}$ can both be known for each component i, a quantitative statement of the liquid-gas partition equilibrium must be given for each of n components. These n additional constraints combine with equation [5.1], the three-dimensional equation [5.3], and the (n-1) independent equations [5.9] to form a closed system of $2n$+3 relations for the $2n$+3 unknowns.

The stated equations depend upon an additional functional relationship: the capillary pressure-saturation relation [5.13], which is considered to be an empirical material-specific relation. The formulation of this functional relationship will be discussed more fully below in Section 7.2, "Relation of capillary pressure to saturation". Moreover, in order that the equations can be parameterised, constitutive relations are required for the phase densities and phase-specific permeabilities (discussed further below under Section 8.1, "Relation of permeability to saturation").

To express the M^2 model for the particular case of PEMFC porous media, it is common to make the following further assumptions:(119)

- Trace gas dissolution (e.g. of reactants or N_2) into the aqueous phase is ignored, so that the liquid phase is pure water ($w_{\mathrm{H_2O,l}} = 1$, $w_{i\neq \mathrm{H_2O,l}} = 0$).(119)
- The liquid water density is assumed constant.
- The gas phase is assumed to obey an ideal gas law, such that the gas phase density is given from the mass fraction of each component can be defined in terms of its partial pressure:

$$\rho_{\mathrm{g}} = \frac{p_{i,\mathrm{g}}}{RT}\left(\sum_i \frac{w_{i,\mathrm{g}}}{M_i}\right)^{-1} \qquad [5.18]$$

- Evaporation-condensation equilibrium for water is applied by setting the partial pressure of water vapour equal to its vapour pressure (p_{vap}, specified as an empirical function of temperature).

$$p_{\mathrm{H_2O,g}} = p_{\mathrm{vap}}(T) \qquad [5.19]$$

Altogether, these assumptions yield the following saturation transport equation:

$$\begin{aligned} &\varepsilon \frac{\partial\left(\rho_{\mathrm{l}} s_{\mathrm{l}} + (1-s_{\mathrm{l}})\dfrac{M_{\mathrm{H_2O}} p_{\mathrm{vap}}}{RT}\right)}{\partial t} + \nabla\cdot\left(\rho\left(\lambda_{\mathrm{l}} + (1-\lambda_{\mathrm{l}})\frac{M_{\mathrm{H_2O}} p_{\mathrm{vap}}}{\rho_{\mathrm{g}} RT}\right)\mathbf{u}\right) \\ &\quad = \varepsilon\nabla\cdot\left(\rho_{\mathrm{g}}(1-s_{\mathrm{l}}) D_{\mathrm{H_2O,g}} M_{\mathrm{H_2O}} \nabla\left(\frac{p_{\mathrm{vap}}}{\rho_{\mathrm{g}} RT}\right)\right) \\ -\nabla\cdot&\left(\left(1-\frac{M_{\mathrm{H_2O}} p_{\mathrm{vap}}}{\rho_{\mathrm{g}} RT}\right)\left(\rho_{\mathrm{l}}\left(-D_{\mathrm{cap}}\nabla s_{\mathrm{l}} - \sum_i D_{\mathrm{sol},i}\nabla w_i - D_T \nabla T\right) + \frac{\kappa_0 \rho}{\mu}\lambda_{\mathrm{l}}\left(\rho_{\mathrm{l}} - \gamma_\rho \rho\right)\mathbf{g}\right)\right) \end{aligned} \qquad [5.20]$$

Additionally, the given assumptions yield (n-1) equations for the (n-1) gas-phase species (other than water):

$$\varepsilon\frac{\partial\left(\rho_{\mathrm{g}}(1-s_{\mathrm{l}}) w_{i,\mathrm{g}}\right)}{\partial t} + \nabla\cdot\left((1-s_{\mathrm{l}})\rho w_{i,\mathrm{g}}\mathbf{u}\right) = \varepsilon\nabla\cdot\left(\rho_{\mathrm{g}}(1-s_{\mathrm{l}}) D_{i,\mathrm{g}}\nabla w_{i,\mathrm{g}}\right) + \nabla\cdot\left(w_{i,\mathrm{g}}\mathbf{j}_{\mathrm{l}}\right) \qquad [5.21]$$

By neglecting the contributions of the Gibbs-Marangoni effect to $\mathbf{j}_{\mathrm{l}}$, and extracting the condensation rate R_{w} as a separate term (thereby generalising again to nonequilibrium conditions), Mazumder and Cole presented the following liquid water saturation equation:(121)

$$\frac{\partial\left(\varepsilon\rho_{\mathrm{l}}s_{\mathrm{l}}\right)}{\partial t}+\nabla\cdot\left(\lambda_{\mathrm{l}}\rho_{\mathrm{l}}\mathbf{u}s_{\mathrm{l}}\right)+\nabla\cdot\left(\frac{\alpha M_{\mathrm{H_2O}}}{F}\mathbf{i}\right)=\nabla\cdot\left(\varepsilon\rho_{\mathrm{l}}D_{\mathrm{cap}}\nabla s_{\mathrm{l}}\right)-\nabla\cdot\left(\frac{\lambda_{\mathrm{l}}\left(1-\lambda_{\mathrm{l}}\right)\kappa\rho\left(\rho_{\mathrm{l}}-\rho_{\mathrm{g}}\right)}{\mu}\mathbf{g}\right)+R_{\mathrm{w}} \quad [5.22]$$

Here, an additional term has been introduced for electroosmotic drag, to be applied only in the CL where electrolyte current is present; α is the electroosmotic drag coefficient and **i** the electrolyte current density. This work also represents the relative mobility of the liquid phase by the following quadratic approximation:(121-123)

$$\lambda_{\mathrm{l}}\approx s_{\mathrm{l}}\left(2-s_{\mathrm{l}}\right) \quad [5.23]$$

5.2 APPLICATION OF THE M^2 MODEL TO PEMFC SIMULATION

The M^2 model as formulated by C.Y. Wang (118) was subsequently applied in an isothermal PEMFC model for the GDL and flow channel, with the aim of determining the onset current density for cathode flooding.(119) A full summary of PEMFC models using the M^2 model is given in the accompanying spreadsheet.

The first 3D formulation of the M^2 model included the gas channels, with the solid regions described as fluid regions of extremely high viscosity.(124) Further significant developments include: application to the MPL (125); non-isothermal flow (126); anisotropic transport properties (127); inhomogeneous thermal contact resistance (128); gas crossover through the membrane (129); compression-dependent tortuosity and permeability of the porous media (130). The M^2 model has proven popular for very large-scale 3D models intended for direct experiment comparison.(131, 132)

5.3 CRITICISM OF THE M^2 MODEL

The M^2 model has been the subject of severe criticism from Gurau et al.(24, 92, 133) The principal criticism is that the combined mass conservation equation [5.1] excludes any reaction source term; hence, it cannot apply to the catalyst layers, where a source or sink of water from the membrane phase will occur on the cathode side due to the ORR. Water sources or sinks may also arise due to electroosmotic drag. This would clearly limit the applicability of the M^2 model to the GDL and MPL, and requires that the catalyst layers be resolved separately from the volumetric two-phase flow equations.(134) It should be noted that applied, approximated forms of the M^2 model equations (as in [5.22]) re-introduce a net mass source term. It appears that after an initial riposte (115), no subsequent discussions of the M^2 model have followed up on this point in detail, although (outside the C.Y. Wang group) its popularity has certainly waned during the 2010s.

More recently, it has been argued that since "[the M^2 model] does not track interfaces rigorously", it is "typically not seen as a net benefit for most PEFC models since they are not limited computationally [except in 3D]".(40) As a general perspective, the advantages of the M^2 model are largely confined to advantages in terms of numerical implementation; as a physical model, it simply adds approximation to the two-fluid model, rather than introducing any alternative treatments. Given the improvement in computational capability as well as software for implementing models such as the two-fluid model, the advantages of the M^2 model are much less appreciable compared to the situation in the mid-2000s, which likely accounts for its less frequent utilisation in contemporary work.

6. REDUCED DIMENSIONALITY MODELS

Given the high aspect ratio of PEMFC porous media (thickness < 1 mm compared to electrode-plane extent of several cm even for lab-scale cells), several researchers have sought methods to reduce the dimensionality of two-phase transport models (114, 135, 136). The uniform two-dimensional case has been described as equivalent to "best case" cell performance (137), in the sense that non-uniformity arising in real, inherently three-dimensional systems will always act to worsen performance.

In a general theoretical work, Qin et al. combined a non-equilibrium thermodynamical theory with volume averaging to construct a coupled system of 2D equations represented the coplanar thin porous layers of different material types (136); various source terms, which may be kinetically limited, describe the transport of material quantities (mass, momentum, energy) between the layers. This theory was applied specifically to PEMFC GDL materials in a work arguing that the fibre and pore dimensions of typical GDL materials are large enough compared to the GDL thickness that a resolved 3D approach should be discouraged, on the basis that no 'representative' volume exists on the length scale much smaller than the GDL itself (138).

Rizvandi et al. similarly considered different porous layers to have a conventional in-plane two-fluid model transport behaviour, while transport between layers can be expressed according to an mass transfer coefficient (114):

$$k_{\mathrm{GDL}\rightarrow\mathrm{MPL}} \propto s_{\mathrm{l,GDL}}^{a_{\mathrm{GDL}}} + s_{\mathrm{l,MPL}}^{a_{\mathrm{MPL}}} \qquad [6.1]$$

where the coefficients a_i are evaluated empirically and were fitted to values ≈ 3.

7. THERMODYNAMIC PROPERTIES AND CONSTITUTIVE RELATIONS FOR PARTIALLY SATURATED POROUS MEDIA

Models based on fundamental fluid dynamics, such as the two-fluid model (Section 4) and M^2 model (Section 5) require surface thermodynamic properties of the liquid-vapour interface, as well as relevant effective porous media transport properties for both the liquid and gas phases. Of these, the capillary pressure-saturation and gas-phase tortuosity-saturation relation have been identified as the most important.(139) In general, effective properties – especially transport properties – will differ between the GDL, MPL, and CL, and may be non-uniform in each region in both the in-plane and through-plane directions. Additionally, the compression of the PEMFC porous media may cause distinguishable effective media properties between the "under-channel" and "under-land" regions with respect to the channels and solid regions ("land") of the adjacent bipolar plate.

Section 7 discusses the (effective) thermodynamic properties of the liquid-gas interface in partially saturated porous media. Section 8 covers the influence of saturation on effective transport properties, as well as the rate of the water evaporation-condensation process.

7.1 BULK PROPERTIES AND BULK INTERFACE THERMODYNAMICS

Two-phase models including a description of liquid water naturally require various material properties of bulk liquid water itself (density, viscosity, etc.). Bulk properties have usually been sourced from standard chemical engineering references and were summarised in early two-phase models, including temperature dependence.(28, 126)

The expression for the water vapour pressure p_{vap} as a function of temperature indicates the position of thermodynamic equilibrium between liquid- and vapour-phase water. A standard polynomial expression for water vapour pressure as a function of temperature has been reported previously.(1) In a partially saturated porous medium, the *Kelvin equation* gives a correction to apparent vapour pressure $p_{\mathrm{vap,app}}$ with respect to the bulk vapour pressure at a plane interface.(139)

$$\ln\left(\frac{p_{\mathrm{vap,app}}}{p_{\mathrm{vap}}}\right) = p_{\mathrm{cap}}\frac{M_{\mathrm{H_2O}}}{RT\rho_{\mathrm{w}}} \qquad [7.1]$$

The vapour pressure is typically considered to be a weak function of total pressure in the relevant operating range for PEMFCs (1–3 bar).

The surface tension of water at an interface with air has been quoted as a linear function of temperature close to room temperature, as follows:(127)

$$\gamma = \gamma_0 - \gamma_1 (T - T_0) \quad [7.2]$$

with γ_0 = 0.077331 N m^{-1}, γ_1 = 1.83 × 10^{-4} N m^{-1} K^{-1}, T_0 = 273.15 K.

Over a wider temperature range, the following nonlinear fit has been reported:(95)

$$\gamma = \gamma_0 \left(1 - \frac{T}{T_0}\right)^{\nu_\gamma} \left(1 - a_\gamma \left(1 - \frac{T}{T_0}\right)\right) \quad [7.3]$$

with γ_0 = 235.8 mN m^{-1}, T_0 = 647.096 K, ν_γ = 1.256, a_γ = 0.625.

For non-isothermal models incorporating water evaporation-condensation, the latent heat of evaporation must be defined. Parameterisation of this quantity will be discussed in a separate review on heat transfer models for PEMFCs.

7.2 RELATION OF CAPILLARY PRESSURE TO SATURATION

A capillary pressure-saturation relation is assumed by both the two-fluid and M^2 theories, and utilised to predict the apparent capillary diffusion coefficient as a function of local saturation. This relation quantifies the role of capillary action on displacement of liquid water within the microscopic pores, which are homogenised in effective porous media models. A wide range of theoretical descriptions have been proposed, and novel experimental techniques have been developed to measure this relation.(10, 13)

By far the most widely applied theoretical relation between capillary pressure and saturation is the *Leverett equation* (140), which originates in soil science and so represents an intrinsically different type of porous solid from the carbon materials encountered in GDLs. As introduced to PEMFC two-phase flow by Wang et al. (119), the Leverett equation relates the capillary pressure to a polynomial "Leverett function" of saturation, $J(s_l)$, which expresses the capillary pressure scaled to the surface tension of the interface, its contact angle on the solid matrix surface (θ_c), and the dry permeability and porosity of the porous medium k.

$$J(s_l) = \frac{p_{cap}}{\gamma \cos\theta_c} \sqrt{\frac{\kappa_{k,0}}{\varepsilon_{k,dry}}} \quad [7.4]$$

Noting the discussion above (Section 4.1) on the sign of the capillary pressure as defined through [4.5] , it should be noted that the Leverett function J is universally positive. In hydrophilic media, $p_{cap} > 0$ and $\underline{\theta_c} < 90°$, so cos $\theta_c > 0$; in hydrophobic media, $p_{cap} < 0$ and $\underline{\theta_c} > 90°$, so cos $\theta_c < 0$. Vynnycky et al. have published a critical discussion of the Leverett equation which appears to be motivated principally by their failure to recognise the notational standard in [4.5].(88)

The overall form of [7.4] has been considered general, but the specific functional form of J depends on the morphology of the pore structure of the material.(18) Berning et al. interpret the Leverett function as an integral across the pore-size distribution (141) and it has been generally recognised that the separation of the saturation-dependence from other properties quantifying the interface thermodynamics, as in [7.4], has much broader validity than any specific choice for the J function.(142)

The most common choice of Leverett function for hydrophilic cases was extracted empirically from Leverett's data by Udell (143), and was used in the original Wang et al. application to PEMFCs:(119)

$$J(s_l) = 1.417(1 - s_l) - 2.120(1 - s_l)^2 + 1.263(1 - s_l)^3 \quad [7.5]$$

As noted above, however, PEMFC porous media are more often hydrophobic or mixed materials. In this case, Pasaogullari and Wang proposed the following alternative, which since its introduction in 2004 has become the much more widely used formulation:(144)

$$J(s_l) = 1.417 s_l - 2.120 s_l^2 + 1.263 s_l^3 \quad [7.6]$$

The latter Leverett function is reported to be used as part of the pre-built two-phase flow model for PEMFCs implemented in the ANSYS FLUENT software.(145) The resulting capillary pressure-saturation is shown in Figure 1.

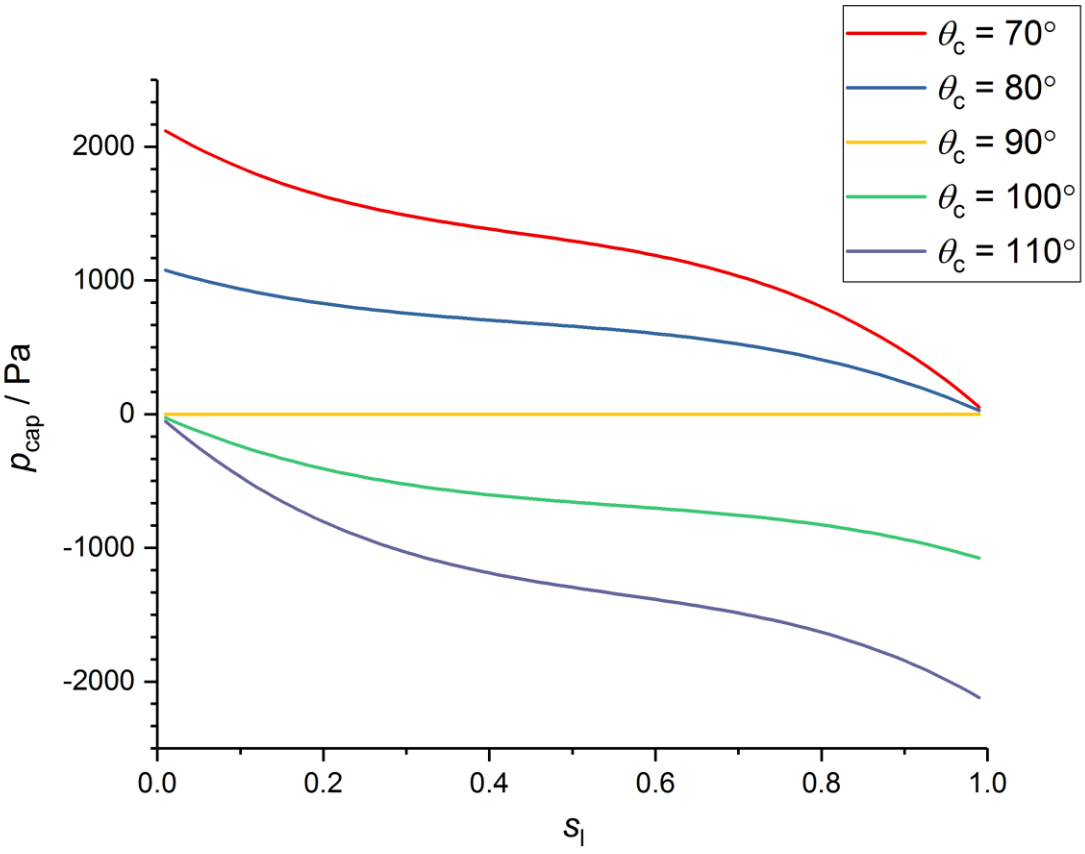

Figure 1: GDL capillary pressure-saturation relation predicted by the Leverett equation with the standard Udell Leverett function for hydrophilic and hydrophobic cases. κ = 10^{-11} m^2, ε = 0.3, γ = 0.065 N m^{-1}.

In one work, the effect of GDL compression due to adjacent land regions has been accounted for empirically by altering the coefficients of the conventional Leverett function:(141)

$$J_{comp}(s_l) = 1.137 s_l - 1.696 s_l^2 + 1.01 s_l^3 \quad [7.7]$$

A number of authors have considered the thermodynamic and transport properties to depend not on absolute saturation, but rather on an effective saturation in which an immobile "residual" or "irreducible" saturation is excluded:(4, 94, 146, 147)

$$s_{l,eff} = \frac{s_l - s_{l,res}}{1 - s_{l,res}} \quad [7.8]$$

Berning et al. argued that the general Leverett function should act on the effective saturation (141), which is considered to arise due to the hydrophilic surfaces within the overall GDL composite volume.(148) They proposed values of $s_{l,res,GDL}$ = 0.2, $s_{l,res,MPL}$ = 0.1, and $s_{l,res,CL}$ = 0.3.

Weber et al. used percolation theory to yield a polynomial expression for the residual saturation, as follows:(6)

$$s_{l,res} = -5.3202\varepsilon_{GDL}^5 + 17.062\varepsilon_{GDL}^4 - 21.706\varepsilon_{GDL}^3 + 13.692\varepsilon_{GDL}^2 - 4.816\varepsilon_{GDL} + 0.9989 \quad [7.9]$$

On the basis of bond correlation probability in a pore network model, Nam et al. proposed $s_{l,res} = 0.11$, which corresponds to $\varepsilon_{GDL} \approx 0.67$ in [7.9].(4)

Kumbur et al. have criticised the Leverett equation due to its origin in studies on soils, which unlike conventional GDL materials exhibit neither mixed wettability nor anisotropy.(146) Their results showed qualitative but not quantitative comparison between the predictions of the Leverett equation and results based on an empirical fit to measured data; specifically, the Leverett equation overpredicts the extent of saturation. More recent studies have criticised the Leverett equation as unsuitable for PEMFC models, since it was derived for hydrophilic media and does not reproduce the hysteresis observed experimentally in GDL material, as discussed further below.(11, 149)

In response to this work, Kumbur et al. presented a "validated Leverett function" for the specific case of SGL 24 series GDL material, using measurements determined by the approach of Gostick et al.(150) (see also "Practical measurement of capillary pressure-saturation relation" below). This yielded a modified Leverett function in the following form, as a function of wt% PTFE (w_{PTFE}) and to be interpreted with $\theta_c = 0°$:

$$J_{K(SGL24)}\left(s_l, w_{PTFE}\right) = \begin{cases} w_{PTFE}\left(0.0469 - 0.00152 w_{PTFE} - 0.0406 s_l^2 + 0.143 s_l^3\right) + 0.0561 \ln s_l, & 0 < s_l < 0.50 \\ w_{PTFE}\left(1.534 - 0.0293 w_{PTFE} - 12.68 s_l^2 + 18.824 s_l^3\right) + 3.416 \ln s_l, & 0.50 \le s_l \le 0.65 \\ w_{PTFE}\left(1.7 - 0.0324 w_{PTFE} - 14.1 s_l^2 + 20.9 s_l^3\right) + 3.79 \ln s_l, & 0.65 < s_l < 1.00 \end{cases} \quad [7.10]$$

The expression at [7.10] represents the combined behaviour of a GDL sample that contains an MPL; the role of the MPL is expressed by the parts of the empirical function at $s_l > 0.5$, while the part at $s_l < 0.5$ represents the standard "GDL" material. Through subsequent studies on compression pressure and temperature, the same researchers extended the use of this expression to the following modified Leverett equation, using the same Leverett function and accounting for thermal expansion of the structure as well as changes in the relative magnitude of surface tension and adhesive forces with temperature:(151)

$$\left(\frac{T_{ref}}{T}\right)^6 2^{0.4\left(\frac{p_{comp}}{p_{ref}}\right)} J_K(s_l) = \frac{p_{cap}}{\gamma}\sqrt{\frac{\kappa_0}{\varepsilon_{GDL}}} \quad [7.11]$$

where $T_{ref} = 293$ K, p_{comp} is compression pressure, and $p_{ref} = 1$ MPa. The compressed porosity is given as a function of uncompressed porosity as:

$$\varepsilon_{GDL} = \varepsilon_{GDL,0}\left(0.1 + \frac{0.9}{1 + 0.0911\left(\frac{p_{comp}}{p_{ref}}\right) - 0.0083\left(\frac{p_{comp}}{p_{ref}}\right)^2}\right) \quad [7.12]$$

for SGL 24 material. Additional empirical expressions for compressed porosity for other materials have also been given.(152)

In extending the experimental approach used to derive these empirical relations to a wider variety of materials, including GDL, MPL and CL materials, LaManna et al. proposed the following general Leverett function form:(37)

$$\begin{aligned} J_{LM}\left(s_l\right) &= a_{LM1} s_l + a_{LM2} s_l^2 + a_{LM3} s_l^3 \\ &= \frac{p_{cap} - p_{cap,ref}}{\gamma}\sqrt{\frac{\kappa_0}{\varepsilon_{GDL}}} \end{aligned} \quad [7.13]$$

Beyond the Leverett function, a number of empirical measurement approaches have been offered. The related semi-empirical *Brooks-Corey equation* [7.14] and van Genuchten equation [7.15] have been explored as an alternative, with comparable scope for empirical fits to measured data.(150, 153-156)

$$p_{\mathrm{cap}} = p_{\mathrm{cap,ref}} \left(1 - s_{\mathrm{l}}\right)^{-\frac{1}{n_{\mathrm{BC}}}} \quad [7.14]$$

$$p_{\mathrm{cap}} = p_{\mathrm{cap,ref}} \left(\left(1 - s_{\mathrm{l}}\right)^{-\frac{1}{m_{\mathrm{vG}}}} - 1 \right)^{\frac{1}{n_{\mathrm{vG}}}} \quad [7.15]$$

The work of Gostick et al. suggested a preference for the van Genuchten equation, especially at low saturation, with the exception of expressions for combined GDL-MPL phases; also the Leverett function was found to give a reasonable fit, without any evidence being noted that it has any uniquely preferable qualities as an empirical form for PEMFC materials.(150) This work also considered the need to use different fitting parameters to the van Genuchten equation for different stages of imbibition and drainage, due to hysteresis.

The van Genuchten equation has also been interpreted as a *J* function, in terms of the Leverett equation:(87, 105)

$$J_{\mathrm{vG}}\left(s_{\mathrm{l}}\right) = J_{\mathrm{vG},0} \left(\left(1 - s_{\mathrm{l}}\right)^{-\frac{1}{m_{\mathrm{vG}}}} - 1 \right)^{\frac{1}{n_{\mathrm{vG}}}} \quad [7.16]$$

Natarajan et al. defined an empirical function of the following form:(28)

$$p_{\mathrm{cap}} = \rho_{\mathrm{w}} g D \left(B + \exp\left(-A\left(s_{\mathrm{l}} - C\right)\right) - \exp\left(+A\left(s_{\mathrm{l}} - C\right)\right)\right) \quad [7.17]$$

The *B* coefficient has no effect on the transport properties in a saturation gradient, as it vanishes in the first derivative:

$$\frac{\partial p_{\mathrm{cap}}}{\partial s_{\mathrm{l}}} = -\rho_{\mathrm{w}} g D A \left(\exp\left(-A\left(s_{\mathrm{l}} - C\right)\right) + \exp\left(+A\left(s_{\mathrm{l}} - C\right)\right)\right) \quad [7.18]$$

These equations can be simplified further to a three-parameter expression as follows:

$$\frac{\partial p_{\mathrm{cap}}}{\partial s_{\mathrm{l}}} = -a_{\mathrm{N}} \sinh\left(b_{\mathrm{N}}\left(s_{\mathrm{l}} - s_{\mathrm{l,ref}}\right)\right) \quad [7.19]$$

The data values in Table 1 have been used in conjunction with these equations.

Table 1 Parameterisation of the Natarajan-Nguyen capillary pressure-saturation relation (Equation [7.17])

Source	*A*	*B*	*C*	*D* / mm
Natarajan et al., original (28)	3.7	21	0.494	0.173
Natarajan et al., revised (93)	3.82	21	0.69	0.133

Originally, Nguyen et al.(157) was cited as a source for the coefficient values, but this paper does not include the given values! Therefore, the experimental origin of these inputs is unclear, and they must be treated as fitted quantities. A handful of subsequent works have employed the same input values, but far fewer than for Leverett equation methods; a direct comparison between the predictions of a

PEMFC model incorporating the Natarajan function or the Leverett function has been given by Birgersson et al.(101)

Ye et al. fitted experimental measurements to a similar but asymmetric exponential fit (five-parameter model), with data in Table 2.(158)

$$p_{\mathrm{cap}} = d\left(\exp\left(-a_1\left(s_{\mathrm{l}} - c\right)\right) - \exp\left(a_2\left(s_{\mathrm{l}} - c\right)\right)\right) + b \qquad [7.20]$$

Table 2 Parameterisation of the Ye-Wang capillary pressure-saturation relation (Equation [7.20])

Parameter	GDL (Toray-060 with 10% PTFE)	CL (thickened)
a_{Y1}	-44.9	-92.36
a_{Y2}	-22.2	-0.0088
b_{Y}	35.6 Pa	-2395 Pa
c_{Y}	0.321	0.567
d_{Y}	-2.09 Pa	-2431 Pa

Other GDL and CL materials have been fitted to the Ye equation [7.20] (17, 35), but the data in question have been identified as outliers compared to other sources (159).

A simple polynomial fit has been used by Gurau et al., with the parameters given in Table 3.(160)

$$p_{\mathrm{cap}} = p_0\left(s_{\mathrm{l}} - s_{\mathrm{l,res}}\right)^{\alpha_{\mathrm{cap}}} \qquad [7.21]$$

Table 3 Parameterisation of the Gurau-Zawodzinski-Mann capillary pressure-saturation relation (Equation [7.21])

Domain	p_0 / Pa	$s_{\mathrm{l,res}}$	α_{cap}
GDL	6260	0.2	-0.05
CL	6240	0.2	-0.025

Koido et al. gave, for carbon paper with 5 wt% PTFE:(161)

$$p_{\mathrm{cap}} / \mathrm{Pa} = \begin{cases} 2.4\times10^6 s_{\mathrm{l}}^2 - 2.5\times10^5 s_{\mathrm{l}}, & 0 \le s_{\mathrm{l}} < 0.05 \\ -10^4 s_{\mathrm{l}} - 6\times10^3, & 0.05 \le s_{\mathrm{l}} < s_{\mathrm{l,max}} \end{cases} \qquad [7.22]$$

The experimental data from Gostick et al. (150) have been fit to the following purely empirical curve:(11)

$$p_{\mathrm{cap}} / \mathrm{Pa} = -4854.1 s_{\mathrm{l}}^2 + 12958 s_{\mathrm{l}}, \quad 0 \le s_{\mathrm{l}} < 0.8 \qquad [7.23]$$

Other experimental data from the same authors (162) have been used as source data, but were overfit (a 17$^{\mathrm{th}}$ order polynomial!).(163) A subsequent fit of these data have been given, including hysteresis, as follows (noting that some of the reported numerical values, repeated in Table 4 do not appear to match the graphical presentation in the paper).(164)

$$p_{\mathrm{cap}} / \mathrm{Pa} = a_0 + a_1 s_{\mathrm{l}} + a_2 s_{\mathrm{l}}^2 + a_3 s_{\mathrm{l}}^3 \qquad [7.24]$$

Table 4 Parameterisation of the Wang et al. capillary-pressure saturation relation based on measurements from Gostick et al. (reduced to 5 s.f.)

	a_0	a_1	a_2	a_3
Imbibition	-1041.9	11312	-2196.0	-760.82
Drainage	-7035.6	71170	124270	73224

Toray 090 material has been characterised according to a similar equation, with data in Table 5.

$$\frac{\partial p_{\mathrm{cap}}}{\partial s_{\mathrm{l}}} / \mathrm{Pa} = b_0 + b_1 s_{\mathrm{l}} + b_2 s_{\mathrm{l}}^2 \qquad [7.25]$$

Table 5 Parameterisation of the Wang et al. capillary-pressure saturation relation for Toray 090 material

PTFE Loading	b_0	b_1	b_2
0%	2.7322×10^4	-1.1634×10^5	1.1487×10^5
20%	5.3907×10^4	-2.1641×10^5	2.08519×10^5

7.3 CAPILLARY DIFFUSION COEFFICIENT

A common formulation of the two-fluid and M[2] models expresses the relation of liquid water flux to saturation gradient using a capillary diffusion coefficient defined from [4.10]. Some early studies assumed that such an equation can be used with a constant (saturation-independent) diffusion coefficient within a defined range of saturation, implying that the capillary pressure is a linear function of saturation in this range.(20, 27, 54, 161-164) A significant difference (up to 4 orders of magnitude) has been noted between empirically determined capillary diffusion coefficients and the implied value from a standard Leverett function at the same level of saturation (117, 165), which is expressed from [4.10] and [7.4] as:

$$D_{\mathrm{cap}} = -\frac{\sqrt{\kappa_{\mathrm{l}}\varepsilon}}{\mu_{\mathrm{w}}} \gamma \cos\theta_{\mathrm{c}} \frac{\partial J}{\partial s_{\mathrm{l}}} \qquad [7.26]$$

Weber and co-authors have consistently criticised formulations using a capillary diffusion coefficient (6, 145) as the ratio of proportionality between water flux and negative saturation gradient, since this "gives the false impression that the saturation is the driving force for fluid flow and that a saturation condition should be used as a boundary condition" (6). Rather, the driving force is *against* the saturation gradient in hydrophobic media, with the accumulation of water increasing droplet radius and thereby lowering capillary pressure.(2)

7.4 PRACTICAL MEASUREMENT OF CAPILLARY PRESSURE-SATURATION RELATION

Various aspects of measurement science for PEMFC porous media, including *ex situ* characterisation, have been reviewed previously.(139, 165) Most experiments have addressed the GDL, which in spite of its complexity – including heterogeneity and anisotropy – has a much simpler and more experimentally accessible structure than the CL.

Mercury intrusion porosimetry has been applied to GDL materials, and used to infer the water capillary pressure-saturation curve by substituting the known contact angle ratios and surface tension for water-air in place of those for mercury-air.(38, 102) In addition to the uncertainty of the latter calculation, traditional mercury intrusion porosimetry is considered inappropriate for gas diffusion media, since it does not distinguish between hydrophilic and hydrophobic structures in the composite porous material.(159, 166) Additionally, the very high pressures required may deform the solid structure.(37, 167)

In the porous diaphragm method, air in the unsaturated sample is displaced by forced water imbibition under pressure; however, the slow recovery of equilibrium in these systems requires a careful cycling approach to reconstruct the capillary pressure-saturation relation reliably for systems with small pores.(161, 168) Nguyen et al. used the same method, under only gravitational pressure to drive water into the sample.(169) It has been noted that these measurements do not display any imbibition-drainage hysteresis, in contrast to subsequent measurements by other methods.(170)

A preferred approach has been to use the "method of standard porosimetry" developed by Volfkovich et al., in which a sample is sandwiched between two standard samples with known capillary pressure-saturation relations.(171) Kumbur et al. pioneered the application of this method to characterisation of PEMFC porous media.(167) Following Gostick et al., octane intrusion is used to access the full pore-size distribution, while deionised water intrusion is used to access hydrophilic pores exclusively.(150) This analysis assumes that:

$$\frac{p_{\text{cap,water|air}}}{p_{\text{cap,octane|air}}} = \frac{\gamma_{\text{water|air}}}{\gamma_{\text{octane|air}}} \qquad [7.27]$$

The method of standard porosimetry was adapted by Fairweather et al., who measured GDL material through a sandwich between a highly hydrophobic and highly hydrophilic material (for example, PTFE and polyvinylidene fluoride, PVDF, respectively), using a microfluidic flow cell to control liquid saturation directly from an external syringe.(172) This study was performed at room temperature, and so did not yield measurement data at practical fuel cell operating temperatures. A similar approach has been taken by using a hydrophilic carbon plate to provide uniform access for liquid water, at uniform pressure.(173) The hydrophilic and hydrophobic materials confine saturation variation to the GDL material; cycling is used with relaxation gaps to ensure equilibrium. The results showed an irreducible (residual) saturation of about 5% by volume, and pronounced hysteresis: GDL material responds hydrophobically to liquid intrusion in the unsaturated state, but hydrophilically to resist gas intrusion once liquid-saturated.(174) This result suggests that "cylindrical channel" models are inadequate to describe the GDL response to flooding. The hysteresis has been associated with the heterogeneous composite structure having mixed wettability, specifically considering an irreversible motion of the phase interface between distinct sites within the composite structure under the different conditions of imbibition and drainage.(175)

Gostick et al. adapted the Fairweather method using very high suction to ensure an initially dry condition; in a detailed study, compression and sample thickness effects were also considered.(162) Measurements under compression have also demonstrated that the extent of compression of the GDL has an appreciable influence on the capillary pressure-saturation relation and its degree of hysteresis, especially by altering the drainage portion of the curve.(176)

The Gostick-Fairweather method of standard porosimetry has also been applied to CL samples, confirming overall hydrophilicity; moreover, the influence of CL cracking on water uptake was shown to be significant in one case.(177) Within these methods, it is difficult to disentangle the water sorption to the ionomer from water uptake in the porous structure: the two methods are measured concurrently. The method of standard porosimetry has been recognised as generally inapplicable in the limit of low saturation, and to be especially unreliable for materials with smaller pore size (MPL and CL materials) where contradictions are revealed with other measurement approaches.(37)
Neutron radiography has also been explored as a method for measuring saturation extent, for the purpose of constructing capillary pressure-saturation relations.(158)

7.5 INTERNAL AND SURFACE CONTACT ANGLES

The internal contact angle upon which the Leverett equation depends is challenging to measure experimentally (11), and as of 2013 it was noted that few studies have provided a comparative treatment across a range of contact angles while using the Leverett equation (88). Given the uncertainty regarding the applicability of capillary pressure-saturation relations derived from the Leverett equation to carbon-based GDL materials, it has been argued that contact angles appearing in models based on the Leverett equation are effectively fitting parameters, and a correlation to physical contact angles of component materials need not be expected.(164)

Contact angles for different PEMFC-relevant materials have been summarised in previous reviews, including the definition of multiple contact angles for the constituent materials within mixed wettability media.(6, 178) PTFE-coated carbon material is expected to be highly hydrophobic. External contact angles in the range 108° – 110° have been reported for bulk PTFE (179) while

external contact angles in the range 80° – 86° have been reported for bare carbon / graphite materials(170, 179). Nam et al. considered the effective contact angle in the composite GDL material as close to 120°.(4)

Values up to 145° for commercial GDLs have been reported from *ex situ* analysis.(11, 102, 110, 180) External sessile drop measurements have yielded values for GDL material in the range from 104° to as high as 164°, and for MPL material in the range from 94° to 143°.(38, 158, 180) The latter external measurements are almost certainly not relevant for evaluating the internal capillary pressure-saturation behaviour, due to the lack of resolution of composite hydrophobic and hydrophilic contributions. Wilhelmy contact angle measurement on single fibres extracted from composite porous media gave a plain fibre contact angle of 80°, contact angles ranging from 82° to 92° for fibres treated in 5 wt% PTFE, and contact angles ranging from 88° to 96° for fibres treated in 20 wt% PTFE.(181) Analysis of alcohol intrusion data using the Washburn equation suggested internal contact angles for the composite structure in the range 100°-110°; the methodology of this analysis is rather uncertain, but at least suggests that internal contact angles are significantly higher than single-fibre contact angles. This work yielded an adapted expression for effective sessile drop contact angle as a function of single-fibre surface contact angle measurements, including a roughness factor R_i:(181)

$$\cos\theta_{\mathrm{c,eff}} = \sum_i R_i \varepsilon_i \cos\theta_{\mathrm{c},i} - \varepsilon_{\mathrm{gas}} \qquad [7.28]$$

This result supports sessile drop contact angles exceeding 120° for PTFE-treated carbon-fibre GDLs. Weber and Newman argue that in the presence of an excess of hydrophilic or hydrophobic pores (> 90% of the majority material), the effective contact angle of composite GDL material is given by the *Cassie-Baxter equation* as a linear cosine weighting:(6)

$$\cos\theta_{\mathrm{c}} = x_{\mathrm{h+}} \cos\theta_{\mathrm{c,h+}} + (1 - x_{\mathrm{h+}}) \cos\theta_{\mathrm{c,h-}} \qquad [7.29]$$

where “h+” and “h-“ denote hydrophilic and hydrophobic pores respectively, with distinct contact angles. This expression has been used subsequently by Chan et al. and Nishiyama et al.(107, 179)
In the case of a composite material in which neither hydrophilic nor hydrophobic pores are in excess, Weber and Newman propose the definition of distinct contact angles for two separate pore networks (denoted +/-), each with its own pore-size distribution and corresponding degree of saturation:(6)

$$\cos\theta_{\mathrm{c,eff,+}} = x_{\mathrm{h+}} \cos\theta_{\mathrm{c,h+}} + (1 - x_{\mathrm{h+}}) \cos\theta_{\mathrm{c,h-}} \qquad [7.30]$$

$$\cos\theta_{\mathrm{c,eff,-}} = (1 - x_{\mathrm{h+}}) \cos\theta_{\mathrm{c,h+}} + x_{\mathrm{h+}} \cos\theta_{\mathrm{c,h-}} \qquad [7.31]$$

Gallagher et al. used the Young-Laplace equation at different assumed contact angles to obtain the fits in Table 6, identifying hysteresis through distinct contact angles in the imbibition and drainage directions.(173)

Table 6 Contact angles proposed for GDL material by Gallagher et al.

	θ_c / ° (Toray 15 μm)	θ_c / ° (Toray 12 μm)
Imbibition	98	96
Drainage	51	59

Using a measured pore size distribution based on a capillary bundle model (6), a contact angle probability density function for Toray TGP-H-090 has been proposed with the statistical properties in Table 7.(174)

Table 7 Contact angle statistical distribution proposed for GDL material by Cheung et al.

Hysteresis Stage	$\theta_{c,\mathrm{mean}}$ / °	σ_θ / °
Imbibition	92	10
Drainage	52	8

7.6 PORE-SIZE DISTRIBUTION ANALYSIS: CAPILLARY PRESSURE AND SATURATION

At the level of an individual cylindrical pore with radius *r* and with a liquid-gas interface at some location along its length, the capillary pressure is given by the Young-Laplace equation as:

$$p_{\mathrm{cap}} = \frac{2\gamma}{r}\cos\theta_{\mathrm{c}} \qquad [7.32]$$

This simple relation has motivated theories of the capillary pressure-saturation relation based on the statistical distribution of pore sizes within the porous medium. Pore-size distribution analysis of GDL material has revealed that the volume fraction is dominated by pores with characteristic size around 10 μm, but also identified a large number of low-volume pores with characteristic size in the 10 nm range.(174) It has been suggested that only large pores are adequately hydrophilic to retain liquid water, and that for an uncompressed sample at room temperature, the volume of connected hydrophilic pores permits a maximum liquid water saturation close to 0.3 for typical GDL material.(167) Compression of materials lowers the modal pore radius, especially for macropores.(152) In simplified models, a Gaussian pore size distribution has been considered.(61)

From the Young-Laplace equation, a critical radius for pore imbibition can be defined as a function of the local capillary pressure:(6)

$$r_{\mathrm{crit}} = \frac{2\gamma\cos\theta_{\mathrm{c}}}{p_{\mathrm{cap}}} \qquad [7.33]$$

This critical radius corresponds to the smallest pore size filled for a hydrophilic pore, or the largest pore size filled for a hydrophobic pore; in the hydrophobic case, both numerator and denominator are negative.

Weber et al. treated the pore-size distribution (as normalised volume) as being described through a sum over *k* unique log-normal distributions, indicating different composite components as well as, where required, an MPL layer:(6, 139)

$$V(r) = \sum_{k} f_{\mathrm{r},k}\left(\frac{1}{r\sigma_k\sqrt{2\pi}}\exp\left(-\frac{1}{2}\left(\frac{\ln\left(\frac{r}{r_{0,k}}\right)}{\sigma_k\sqrt{2}}\right)^2\right)\right) \qquad [7.34]$$

The saturation for a particular capillary pressure is then evaluated by integrating $V(r)$ in the range 0 to r_{crit} for hydrophilic materials, and in the range r_{crit} to ∞ for hydrophobic materials. This yields the following analytical expression, for j = +/- for the hydrophilic / hydrophobic fractions of the mixed wettability composite:

$$s_{\mathrm{l}} = \sum_{j} x_j \sum_{k} \frac{f_{\mathrm{r},k}}{2}\left(1+\phi_j\ \mathrm{erf}\left(\frac{\ln\left(\frac{r_{\mathrm{crit},k}}{r_{0,k}}\right)}{\sigma_k\sqrt{2}}\right)\right) \qquad [7.35]$$

where φ_j = +1 for hydrophilic pores and = -1 for hydrophobic pores. Thus, since the $r_{\mathrm{crit},k}$ are functions of capillary pressure from [7.33], a capillary pressure-saturation relation has been expressed. From the pore-size distribution of the unsaturated pores, an average pore radius for Knudsen diffusion may also be inferred.(6)

A further extension of this model considered that not only pore size but also contact angle should be treated as a continuous probability distribution, such that averaged properties of the porous medium

are expressed by double integration across both distributions.(139) The contact angle distribution is described according to a Gaussian distribution; since this contact angle distribution cannot be directly measured, it is characterised by fitting to a measured capillary pressure-saturation relation. Different fitted values, including hysteresis with respect to imbibition and drainage, are given in the literature for SGL and Toray GDLs as well as a typical MPL material.(139)

8. EFFECTIVE TRANSPORT AND KINETIC PROPERTIES OF PARTIALLY SATURATED POROUS MEDIA

8.1 RELATION OF PERMEABILITY TO SATURATION

The liquid-phase and gas-phase permeabilities for use in two-phase Darcy's law models are typically correlated to the dry (absolute) permeability κ_0 of the porous matrix according to a polynomial expression in saturation:

$$\kappa_\mathrm{l} = \kappa_0 s_\mathrm{l}^{n_\kappa} \qquad [8.1]$$

$$\kappa_\mathrm{g} = \kappa_0 \left(1 - s_\mathrm{l}\right)^{n_\kappa} \qquad [8.2]$$

Natarajan et al. proposed a linear correlation with a small offset at $s_\mathrm{l} = 0$, for numerical stability reasons:(28)

$$\kappa_\mathrm{l} = \kappa_{\mathrm{sat,l}} \left(s_\mathrm{l} + 0.01\right) \qquad [8.3]$$

The cubic relation ($n_\kappa = 3$, sometimes called the "Wyllie model" (146)) is the approach most often used in 'conventional' two-fluid models with a standard Leverett function (see accompanying summary spreadsheet), including in the standard implementation in ANSYS FLUENT (145). The cubic relation was popularised by its use alongside the standard Leverett function form by Udell, drawing on the legacy of various earlier works in soil science.(143) Like the standard Leverett function, the cubic permeability correlation was derived for non-consolidated sands, with no intrinsic validity for GDL material.(146) Olapade et al. report that a cubic correlation can be derived based on a percolation theory through cut and rejoined tubes.(163) The cubic correlation has been supported using X-ray tomography data for the structure of Toray GDL samples.(182)

Since 2007, works from the C.Y. Wang group use a quartic correlation ($n_\kappa = 4$) (183), which was derived in the limit of high saturation of the hydrophobic component by Corey (184). The Nguyen group has used a super-quartic correlation ($n_\kappa = 4.5$).(19)

As carbon fibres tend to align with each other in manufactured GDL media, κ_0 is expected to be anisotropic for standard GDL materials, with a higher in-plane permeability.(127) This anisotropy has been expressed in some previous modelling studies.(141, 185) Zhang et al. expressed the permeability in the Leverett function as the vectorial sum of two anisotropic permeabilities:(27)

$$\kappa_\mathrm{ave} = \frac{\sqrt{\left(\kappa_\parallel \nabla p_\mathrm{l} \cdot \mathbf{t}_1\right)^2 + \left(\kappa_\parallel \nabla p_\mathrm{l} \cdot \mathbf{t}_2\right)^2 + \left(\kappa_\perp \nabla p_\mathrm{l} \cdot \mathbf{n}\right)^2}}{\left|\nabla p_\mathrm{l}\right|} \qquad [8.4]$$

where the unit vectors $\mathbf{t}_1$ and $\mathbf{t}_2$ are in the GDL plane where the permeability component is $\kappa_\parallel$, and the unit vector $\mathbf{n}$ is normal to the GDL plane, where the permeability component is $\kappa_\perp$.

Gostick et al., Quick et al. and Hussaini et al. have provided detailed databases of measurements for the absolute and relative permeabilities of GDL materials, affirming the anisotropy of the materials in which in-plane permeability exceeds through-plane permeability.(25, 32, 186) A fit to some of these data has suggested $n_\kappa = 2.16$ for liquid permeability.(146) Hussaini et al. recommend the use of a cubic correlation for the in-plane permeability of the gas phase with a carbon cloth GDL, while for a carbon paper GDL, a quartic relation in $\left(1 - s_\mathrm{l}^2\right)$ is recommended.(25) The same work recommends that the

quartic relation be used for the in-plane permeability of the water phase, in all types of GDL material. Experimental measurements on Toray 090 have conversely suggested $n_\kappa = 5$ for an untreated sample and $n_\kappa = 2$ for a 20% PTFE sample.(165)

Measurements using the "porous diaphragm" method on one sample suggested:(161)

$$\frac{\kappa_\mathrm{l}}{\kappa_0} = 1.089\left(s_\mathrm{l}^{1.5} - 1\right) + 1 \qquad [8.5]$$

$$\frac{\kappa_\mathrm{g}}{\kappa_0} = \left(1 - s_\mathrm{l}\right)^5 \qquad [8.6]$$

The Corey, Brooks-Corey and van Genuchten equations additionally offer semi-empirical permeability expressions. The van Genuchten permeability dependence has been quoted as:(154)

$$\frac{\kappa_\mathrm{l}}{\kappa_0} = s_\mathrm{l}^{\gamma_\mathrm{vG}} \left(1 - \left(1 - s_\mathrm{l}^{\frac{1}{m_\mathrm{vG}}} \right)^{m_\mathrm{vG}} \right)^2 \qquad [8.7]$$

while the gas permeability follows the same equation with s_l substituted by $(1\text{-}s_\mathrm{l})$. Empirical exponents have been used as $\gamma_\mathrm{vG} = 0.5$ and $m_\mathrm{vG} = 0.95$.(154)

In the "bundle of parallel pores" theory, the permeability is calculated from the capillary pressure-saturation relation as follows (so-called "Burdine functions"):(102, 187)

$$\kappa_\mathrm{l} = \kappa_0 s_\mathrm{l,eff}^2 \frac{\int_0^{s_\mathrm{l}} \frac{ds_\mathrm{l}'}{p_\mathrm{cap}^2\left(s_\mathrm{l}'\right)}}{\int_0^1 \frac{ds_\mathrm{l}'}{p_\mathrm{cap}^2\left(s_\mathrm{l}'\right)}} \qquad [8.8]$$

$$\kappa_\mathrm{g} = \kappa_0 \left(1 - s_\mathrm{l,eff}\right)^2 \frac{\int_{s_\mathrm{l}}^1 \frac{ds_\mathrm{l}'}{p_\mathrm{cap}^2\left(s_\mathrm{l}'\right)}}{\int_0^1 \frac{ds_\mathrm{l}'}{p_\mathrm{cap}^2\left(s_\mathrm{l}'\right)}} \qquad [8.9]$$

These expressions predict that the sum of liquid-phase and gas-phase permeabilities in a partially saturated porous medium is less than the dry permeability, due to percolation limitations from pore connectivity.

Alternatively, the more general "Mualem functions" have been defined to relate capillary pressure-saturation relation to permeability:(188)

$$\kappa_\mathrm{l} = \kappa_0 s_\mathrm{l,eff}^{\eta_\mathrm{M}} \left(\frac{\int_0^{s_\mathrm{l}} \frac{ds_\mathrm{l}'}{p_\mathrm{cap}\left(s_\mathrm{l}'\right)}}{\int_0^1 \frac{ds_\mathrm{l}'}{p_\mathrm{cap}\left(s_\mathrm{l}'\right)}} \right)^2 \qquad [8.10]$$

$$\kappa_\mathrm{g} = \kappa_0 \left(1 - s_\mathrm{l,eff}\right)^{\eta_\mathrm{M}} \left(\frac{\int_{s_\mathrm{l}}^1 \frac{ds_\mathrm{l}'}{p_\mathrm{cap}\left(s_\mathrm{l}'\right)}}{\int_0^1 \frac{ds_\mathrm{l}'}{p_\mathrm{cap}\left(s_\mathrm{l}'\right)}} \right)^2 \qquad [8.11]$$

The Burdine functions have been described as appropriate in combination with the Brooks-Corey equation for p_{cap}, while the Mualem functions combine appropriately with the van Genuchten equation.(10) The significant proliferation of expressions arising from the different assumptions contained in these methods requires further work to unify and to relate to established standards in the historical literature on porous media.

A significant discrepancy (several orders of magnitude) has been noted between measured values of absolute permeability for GDL materials (close to 10^{-12} m^2) and the values required to reproduce pressure drops observed *in situ*.(189, 190) It has been noted experimentally that increased PTFE loading lowers the dry porosity and increases the dry permeability of GDL materials; however, it does not appear that any attempts have been made to describe this effect mathematically.(38)

8.2 PORE-SIZE DISTRIBUTION ANALYSIS: PERMEABILITY AND INTERFACIAL SURFACE AREA

Using a parallel pore model followed by a "cut-and-join" method, and then expanding the integrals, gives the following rather verbose expressions for permeability in each phase:(6)

$$\kappa_{\mathrm{l}} = \kappa_0 \frac{s_{\mathrm{l,eff}}^2}{2} \sum_j x_j \sum_k f_{\mathrm{r},k} \left(1 + \theta_j \, \mathrm{erf} \left(\frac{\ln\left(\frac{r_{\mathrm{c},j}}{r_{0,k}} \right)}{\sigma_k \sqrt{2}} - \sigma_k \sqrt{2} \right) \right) \qquad [8.12]$$

$$\kappa_{\mathrm{g}} = \kappa_0 \frac{\left(1 - s_{\mathrm{l,eff}}\right)^2}{2} \sum_j x_j \sum_k f_{\mathrm{r},k} \left(1 - \theta_j \, \mathrm{erf} \left(\frac{\ln\left(\frac{r_{\mathrm{c},j}}{r_{0,k}} \right)}{\sigma_k \sqrt{2}} - \sigma_k \sqrt{2} \right) \right) \qquad [8.13]$$

The original work introducing [8.12]-[8.13] treated the dry permeability as an empirical constant. Following the pore-size distribution analysis introduced in Section 7.6, however, the dry permeability has more recently been expressed directly from the pore-size distribution, using the Hagen-Poiseuille equation to give:(178)

$$\kappa_0 = \frac{1}{8} \left(\frac{\varepsilon_{\mathrm{dry}}}{\lambda_{\mathrm{PSD}}} \right)^2 \sum_k r_{0,k}^2 \, f_{\mathrm{r},k} \exp\left(-2\sigma_k^2 \right) \qquad [8.14]$$

Here, λ_{PSD} is an empirical representation of the degree of interconnectivity of pores, used in the "cut-and-join" theory. Fits to data for GDL materials have suggested a range $1 < \lambda_{\mathrm{PSD}} \leq 2$.(178) Combining [8.14] with [8.12] gives:(178)

$$\kappa_{\mathrm{l}} = \kappa_0 \frac{s_{\mathrm{l,eff}}^2}{2} \frac{\sum_j x_j \sum_k r_k^2 \exp\left(-2s_k^2 \right) f_{\mathrm{r},k} \left(1 + \theta_j \, \mathrm{erf} \left(\frac{\ln\left(\frac{r_{\mathrm{c},j}}{r_{0,k}} \right)}{s_k \sqrt{2}} - s_k \sqrt{2} \right) \right)}{\sum_j x_j \sum_k r_{0,k}^2 \exp\left(-2s_k^2 \right) f_{\mathrm{r},k}} \qquad [8.15]$$

and similarly for the relative gas permeability. These expressions closely resemble the cubic $n_\kappa = 3$ empirical expression (6), and have been subsequently extended to consider a range of contact angles (139).

Secanell and co-workers derived the liquid-gas interfacial surface area (per unit composite volume) using a probability distribution for the cross-sectional area of liquid-invaded pores multiplied by the remaining cross-section:(178)

$$a_{\mathrm{vol}}\left(r\right)dr = \frac{1}{4r}\left(1-\left(\frac{1}{4r\sum_{k}\frac{f_{\mathrm{r},k}\exp\left(\frac{\sigma_k^2}{2}\right)}{4r_{0,k}}}\right)\right) \qquad [8.16]$$

Integrating with respect to r across the defined probability distribution gives:

$$a_{\mathrm{vol}} = \sum_{j} x_j \sum_{k} f_{\mathrm{r},k}\frac{\exp\left(\frac{\sigma_k^2}{2}\right)}{8r_{0,k}}\left(1+\theta_j \mathrm{erf}\left(\frac{\ln\left(\frac{r_{\mathrm{crit}}}{r_{0,k}}\right)}{\sigma_k\sqrt{2}}+\frac{\sigma_k\sqrt{2}}{2}\right)\right) \qquad [8.17]$$

8.3 GAS-PHASE TORTUOSITY DUE TO LIQUID WATER

The "blocking" effect of liquid water on gas-phase diffusion towards the catalyst layer contributes to transport limitations on PEMFC performance. This effect is typically described by means of a saturation-dependent tortuosity for diffusion of gas-phase species, where tortuosity (τ) is defined in terms of the ratio of observed to bulk diffusivity, scaled by the porosity of the medium:

$$\frac{D_{i,\mathrm{eff},k}}{D_i} = \frac{\varepsilon_k}{\tau_k} \qquad [8.18]$$

Measurement of the dry tortuosity of typical GDL materials has been discussed extensively elsewhere.(191) The bulk diffusivity may be modified in the microporous part of the pore-size distribution due to Knudsen diffusion, which expresses the altered diffusion phenomena occurring in systems where the solid-solid separation (i.e. pore diameter) is comparable to the mean free path (≈ 75 nm at 1 atm, 80 °C). The quantitative theory of Knudsen diffusion was reviewed previously.(3) Although it is a two-phase phenomenon, the saturation-dependence of gas-phase tortuosity explicitly affects the transport of reactant gases. Under isothermal conditions and under saturation of the vapour phase with water (that is, assuming evaporation-condensation equilibrium), the water activity remains constant through the gas diffusion layer, and therefore no gas-phase diffusion of water vapour can occur.(120)

A traditional approach to quantify diffusional limitations from liquid water is to express the gas-phase tortuosity with a Bruggeman-type relation dependent on saturation:

$$D_{i,\mathrm{eff},\mathrm{GDL}} = D_i\left(\varepsilon_{\mathrm{GDL}}\left(1-s_{\mathrm{l}}\right)\right)^{n_D} \qquad [8.19]$$

Here, the quantity n_D is sometimes termed the "pore blockage exponent".(192) While many models follow the classical Bruggeman theory in which n_D = 3/2 (6, 193), measured values are typically significantly higher (n_D > 3) (84, 139, 194) and the relation may be suitable only for lower saturations at which significant blockage of the pore network has not occurred.(194) Das et al. reviewed the Bruggeman theory and its extensions for both GDL and CL materials.(195)

Weber and Newman argued that a residual gas-phase saturation must be considered:

$$D_{i,\mathrm{eff},\mathrm{GDL}} = D_i\left(\varepsilon_{\mathrm{GDL}}\left(s_{\mathrm{g,res}}-s_{\mathrm{l}}\right)\right)^{n_D} \qquad [8.20]$$

where

$$s_{\mathrm{g,res}} = 1 - s_{\mathrm{l,res}}, \quad s_{\mathrm{l,res}} \leq 0.15$$
$$s_{\mathrm{g,res}} = 0.85, \quad s_{\mathrm{l,res}} > 0.15 \qquad [8.21]$$

A more general Bruggeman-type expression for effective diffusivity in any given porous medium has been proposed, in which different exponents are applied for the saturation and (dry) porosity contributions:(33, 196)

$$\frac{D_{i,\mathrm{eff,GDL}}}{D_i} = \varepsilon^{m_D} \left(1 - s_{\mathrm{l}}\right)^{n_D} \qquad [8.22]$$

Based on experimental data from García-Salaberri et al.(197, 198), Zhou et al. have suggested (for the GDL) $m_D = 1$, $n_D = 2.5$ in-plane, and $n_D = 3.5$ through-plane.(178) More recently, the compilation of data from Balasubramanian and Weber suggested $m_D = 3.6$ (149), while Wang et al. suggested $m_D = n_D = 4.0$ and provided a useful summary of other measurements.(33)

Pasaogullari et al. defined a partially anisotropic Bruggeman exponent for dry porosity as follows:(127)

$$\frac{D_{i,\mathrm{eff,GDL}}}{D_i} = \varepsilon_{\mathrm{GDL}} \left(\frac{\varepsilon_{\mathrm{GDL}} - p_{\mathrm{bc}}}{1 - p_{\mathrm{bc}}} \right)^{m_{D,i}} \qquad [8.23]$$

where p_{bc} is a correlation probability conventionally set to 0.11 and $m_{D,\parallel} = 0.521$, $m_{D,\perp} = 0.785$.(4, 75, 199) This correlation probability has been identified as equivalent to a limiting volume fraction $\varepsilon_{\mathrm{lim}}$, as follows:(27, 31, 200)

$$\frac{D_{i,\mathrm{eff,GDL}}}{D_i} = \varepsilon_{\mathrm{GDL}} \left(1 - s_{\mathrm{l}}\right) \left(\frac{\varepsilon_{\mathrm{GDL}} \left(1 - s_{\mathrm{l}}\right) - \varepsilon_{\mathrm{lim}}}{1 - \varepsilon_{\mathrm{lim}}} \right)^{m_{D,p}} \qquad [8.24]$$

A further slight variation has been given by Nam et al.:(4)

$$\frac{D_{i,\mathrm{eff,GDL}}}{D_i} = \varepsilon_{\mathrm{GDL}} \left(1 - s_{\mathrm{l}}\right)^2 \left(\frac{\varepsilon_{\mathrm{GDL}} - \varepsilon_{\mathrm{lim}}}{1 - \varepsilon_{\mathrm{lim}}} \right)^{m_{D,p}} \qquad [8.25]$$

Based on a pore network model, Dawes et al. derived:(75)

$$\frac{D_{i,\mathrm{eff,GDL}}}{D_i} = \left(\frac{\varepsilon_{\mathrm{GDL}} - p_{\mathrm{bc}}}{1 - p_{\mathrm{bc}}} \right)^{m_D} \left(\frac{\left(1 - s_{\mathrm{l}}\right) - p_{\mathrm{bc}}}{1 - p_{\mathrm{bc}}} \right)^{n_D} \qquad [8.26]$$

with $p_{\mathrm{bc}} = 0.11$ and $m_D = n_{\mathrm{D}} = 0.9$.

Through a fractal model including Knudsen diffusion, the tortuosity has been defined as follows for a pore of radius r_{pore}:(201)

$$\tau\left(r_{\mathrm{pore}}\right) = \left(\frac{d_{\mathrm{GDL}}}{2 r_{\mathrm{pore}}} \right)^{f_\tau - 1} \qquad [8.27]$$

where f_τ is a tortuosity fractal dimension. Now a probability distribution is set:

$$P\left(r > r_{\mathrm{pore}}\right) \propto \left(\frac{r_{\mathrm{pore,max}}}{r_{\mathrm{pore}}} \right)^{f_A} \qquad [8.28]$$

where f_A is an area fractal dimension. These two fractal dimensions with the minimum and maximum capillary radii are then used to express the effective oxygen diffusivity by taking a weighted average of the effective diffusivity at a specific pore radius across the distribution of pore radii. The diffusion coefficient as a function of pore radius is expressed as a combination of conventional and Knudsen

diffusion coefficients, including the effects of water saturation in terms of critical radius, with filled pores being treated as completely blocking to oxygen transport. Since the resulting expressions are quite complicated, they are not reproduced here in full. Good agreement with experimental data is established by using the fractal dimensions as additional fitting parameters; fits suggested $f_\tau = 1.1447$ and $f_A = 1.9669$.(201)

Wang et al. collated experimental measurements of gas-phase tortuosity in the MPL according to the same formulation as [8.22], and proposed that if Knudsen diffusion is excluded, $m_D = n_D = 2$, but if Knudsen diffusion is incorporated in the theoretical model, $m_D = n_D = 4$.(33)
In the catalyst layer, the following expression has been suggested:(202)

$$\frac{D_{i,\mathrm{eff,CL}}}{D_i} = \left(1 - s_\mathrm{l}\right)^{m_D} \left(\frac{\varepsilon_{\mathrm{CL,dry}} - \varepsilon_\mathrm{lim}}{1 - \varepsilon_\mathrm{lim}} \right)^{n_D} \qquad [8.29]$$

wherein a critical percolation limit on saturation exists, at which gas-phase diffusion falls to zero:

$$s_{\mathrm{l,crit,diff}} = 1 - \frac{\varepsilon_\mathrm{lim}}{\varepsilon_{\mathrm{CL,dry}}} \qquad [8.30]$$

8.4 EVAPORATION-CONDENSATION RATE

In models where saturation is explicitly resolved as a function of position through partially saturated porous media, there is a need either to impose thermodynamic equilibrium for the evaporation-condensation phase change of water, or to quantify the rate of the evaporation-condensation process. The spatial variation of evaporation and condensation rate has been implicated as a greater net contributor to liquid water transport than the direct phenomenon of capillary diffusion.(32) Some pseudo-two-phase treatments allow evaporation-condensation to proceed at the membrane or catalyst layer, but assume that the gas diffusion layer has separate liquid- and gas-transporting regions, and so is not a site of phase change.(78, 203)

Given the assumption that the available liquid-gas interfacial area controls the observed evaporation-condensation rate (i.e. there is no kinetic limitation to the process), the typical pore size in GDL materials suggests that evaporation-condensation equilibrium is maintained locally in GDL materials, to a good approximation.(39, 204, 205) For this reason, Ferng et al. assumed that equilibrium holds wherever liquid water is present; if the liquid water phase is assumed to always be present, this requires that the partial pressure of water vapour must equal the vapour pressure.(73) Then, the saturation level is an explicit function of the total water mass fraction $w_{\mathrm{H_2O}}$ (combining both phases):

$$s_\mathrm{l} = \frac{\rho_\mathrm{g}\left(w_{\mathrm{H_2O}} - w_{\mathrm{H_2O,g,eq}}\right)}{\rho_\mathrm{l}\left(1 - w_{\mathrm{H_2O}}\right) + \rho_\mathrm{g}\left(w_{\mathrm{H_2O}} - w_{\mathrm{H_2O,g,eq}}\right)} \qquad [8.31]$$

$$w_{\mathrm{H_2O,g,eq}} \equiv \frac{\rho_{\mathrm{H_2O,vap,eq}}}{\rho_{\mathrm{H_2O,vap,eq}} + \rho_{\mathrm{g,non\text{-}H_2O}}} \qquad [8.32]$$

The application of an equilibrium method is unclear in cases where some regions may be completely dry (single-phase regions). A “pseudo-phase equilibrium” approach has been recommended to address this problem while avoiding interface tracking.(86) In this model, the water vapour partial pressure tends towards the vapour pressure according to an empirical metric of deviation δ_eq:

$$\frac{p_{\mathrm{H_2O}}}{p_\mathrm{vap}} = 1 - \exp\left(\frac{\ln \delta_\mathrm{eq}}{\delta_\mathrm{eq}} s_\mathrm{l} \right) \qquad [8.33]$$

As $\delta_\mathrm{eq} \rightarrow 0$, so a precise equilibrium condition is recovered. Yin et al. used [8.33] with constant values for δ_eq based on numerical convergence (i.e. set as low as possible), using values 0.01/0.03 for 1D/2D. This approach can be understood as a smoothing of the thermodynamic prediction, so that the vapour

phase remains unsaturated at low overall degree of water saturation. Yin et al. have subsequently written simply:(206)

$$\frac{p_{\mathrm{H_2O}}}{p_{\mathrm{w,sat}}} = \left(s_{\mathrm{l}}\right)^{\frac{1}{n_{\mathrm{eq}}}} \qquad [8.34]$$

with the absurd input $n_{\mathrm{eq}} = 600$ presumably accounting for the reported high degree of numerical ill-conditioning of the simulation in this case. It is possible, but has not yet been explored in the literature, that a more physically motivated "pseudo-phase equilibrium" approach could be derived, in order to retain the general Hsuen-Yin approach of enforcing equilibrium except at trace saturations where an interfacial surface area-limited rate prevails.

Most two-fluid models (especially 'standard models' with a conventional Leverett function and cubic permeability-saturation relations, such as the PEMFC model in ANSYS FLUENT (145)) follow the work of He et al. to express the evaporation and condensation rates per total porous material volume as linear functions of deviation of the water partial pressure from its equilibrium value:(207)

$$R_{\mathrm{w,g}\to\mathrm{l}} = k_{\mathrm{c}} M_{\mathrm{H_2O}} c_{\mathrm{w,g}} \frac{p_{\mathrm{H_2O}} - p_{\mathrm{vap}}}{p_{\mathrm{A}}}, \quad p_{\mathrm{H_2O}} > p_{\mathrm{vap}} \qquad [8.35]$$

$$R_{\mathrm{w,l}\to\mathrm{g}} = -k_{v} M_{\mathrm{H_2O}} c_{\mathrm{w,l}} \left(p_{\mathrm{vap}} - p_{\mathrm{H_2O}}\right), \quad p_{\mathrm{H_2O}} \le p_{\mathrm{vap}} \qquad [8.36]$$

The apparent molar concentrations per total porous material volume are given as follows:

$$c_{\mathrm{w,g}} = \varepsilon_{i,\mathrm{dry}} \left(1 - s_{\mathrm{l}}\right) \frac{p_{\mathrm{H_2O}}}{RT} \qquad [8.37]$$

$$c_{\mathrm{w,l}} = \varepsilon_{i,\mathrm{dry}} s_{\mathrm{l}} \frac{\rho_{\mathrm{w}}}{M_{\mathrm{H_2O}}} \qquad [8.38]$$

In the original work, values of the rate constants of $k_{\mathrm{c}} = 100\ \mathrm{s^{-1}}$ and $k_{\mathrm{v}} = 100\ \mathrm{atm^{-1}\ s^{-1}}$ were used, which were reported to yield close to thermodynamically controlled behaviour (207); subsequent parameterisations were recently summarised by Yin et al.(206) Meng et al. suggested that $k_{\mathrm{c}} = 5000\ \mathrm{s^{-1}}$ is consistent with experiment, implying only negligible deviation from thermodynamic equilibrium.(205) Yin et al. pointed out that, for high values of the rate constants, the approach in the He evaporation-condensation equations necessarily (trivially) tends towards the same behaviour as pseudo-phase equilibrium. Additionally, the particular choice of boundary conditions can cause localisation of the phase change to different parts of the GDL, without appreciable differences to the overall polarisation performance.(206, 208)

Shah et al. placed the He equations into a "differentiable form" (103, 209) by eliminating the logical switch functions, although their resulting expressions are singular at $p_{\mathrm{H2O}} = p_{\mathrm{w,sat}}$. Nam et al. proposed factorising the gas-liquid interfacial area from the rate constants in the He equations.(4) Unfortunately, the work also leaves open the possibility to implicitly set the products $k_{\mathrm{c}} c_{\mathrm{w,g}}$ and $k_{\mathrm{v}} c_{\mathrm{w,l}}$ as constants by defining the interfacial area as saturation-independent; for instance, Nam et al. use $a_{\mathrm{vol,lg}} = 1000\ \mathrm{m^{-1}}$ as a fixed reference value. This approach may be valid in narrow ranges of saturation but if applied generally, as by some subsequent authors (65, 210), it eliminates any interfacial area dependence and may lead to an ill-conditioned problem or an evaporation rate expression that does not go to zero for zero saturation.

Weber and Newman constructed a linear equation in the difference of chemical potential of water in the two phases, which is similar to the He equation but expresses the volumetric interfacial area as a prefactor, and includes a Kelvin equation correction (from [7.1]) to the value of the vapour pressure p_{vap}.(6) This approach has been subsequently combined with a pore-size distribution-based specific surface area.(178) The volumetric interfacial area appears to have been neglected in the subsequent

work of Balliet and Newman (211), leading to similar issues to those noted above on constant prefactors in factorisation of the He equations.

On the basis of an empirical fit to pore network modelling results as well as experimental data, Bapat et al. evaluated liquid-gas interfacial area according to:(105)

$$a_{\mathrm{vol}} = a_{\mathrm{vol,max}} \pi \left(\varepsilon_{\mathrm{l}} \varepsilon_{\mathrm{g}}^2 \right)^{0.6} \qquad [8.39]$$

with $a_{\mathrm{vol,max}}$ = 265 m^{-1}.

The "Langmuir formula" for evaporation rate constant was combined with an expression assuming spherical water droplets, to give:(87)

$$R_{\mathrm{w}} = \sqrt{\frac{M_{\mathrm{H_2O}} RT}{2\pi}} \frac{f_{\mathrm{vap}}}{d_{\mathrm{pore}}} \left(c_{\mathrm{H_2O,g}} - c_{\mathrm{H_2O,g,sat}} \right) \qquad [8.40]$$

with d_{pore} = 1 μm (representative of GDL pore size) and

$$h_{\mathrm{vap}} = \begin{cases} s_{\mathrm{l}}^{2/3} & c_{\mathrm{H_2O,g}} < c_{\mathrm{H_2O,g,sat}} \\ \left(1 - s_{\mathrm{l}}\right)^{2/3} & c_{\mathrm{H_2O,g}} > c_{\mathrm{H_2O,g,sat}} \end{cases} \qquad [8.41]$$

Some works define the reaction rate in terms of a dimensionless Sherwood number ($\mathrm{Sh_g}$). For instance:(212, 213)

$$R_{\mathrm{w}} = \rho_{\mathrm{vap}} a_{\mathrm{gl}} D_{\mathrm{H_2O,g}} \frac{\mathrm{Sh_g}}{d_{\mathrm{drop}}} \ln\left(1 + \mathrm{B_m}\right) \qquad [8.42]$$

where writing $a_{\mathrm{gl}} = 3s_{\mathrm{l}}/r_{\mathrm{drop}}$ according to a spherical droplet model yields

$$R_{\mathrm{w}} = \mathrm{Sh_g} \frac{6\rho_{\mathrm{vap}} D_{\mathrm{H_2O,g}}}{d_{\mathrm{drop}}^2} \ln\left(1 + \mathrm{B_m}\right) \qquad [8.43]$$

In this formula, $\mathrm{B_m}$ is the Spalding number, although the work does not suggest values for this quantity. The Sherwood number can be assessed from the Reynolds number Re for gas flow with respect to water droplet velocity and size, and the Schmidt number for water vapour in the gas flow:

$$\mathrm{Sh_g} \approx 2 + 0.69 \mathrm{Re}^{1/2} \mathrm{Sc}_{\mathrm{H_2O}}^{1/3} \qquad [8.44]$$

The expression [8.43] does not consider the position of direction of equilibrium; although this has been included in a similar expression:(156)

$$R_{\mathrm{w}} = \mathrm{Sh_g} \frac{6 M_{\mathrm{H_2O}} \rho_{\mathrm{vap}} D_{\mathrm{H_2O,g}}}{d_{\mathrm{drop}}^2} \left(w_{\mathrm{H_2O}} - w_{\mathrm{H_2O,sat}} \right) \qquad [8.45]$$

Berning and co-workers gave a comparable expression but with an adapted driving force:(210)

$$R_{\mathrm{w,l\rightarrow g}} = \mathrm{Sh_g} \frac{6 M_{\mathrm{H_2O}} \rho_{\mathrm{vap}} D_{\mathrm{H_2O,g}}}{d_{\mathrm{drop}}^2} \frac{p_{\mathrm{H_2O}} - p_{\mathrm{H_2O,sat}}}{p_{\mathrm{A}} - p_{\mathrm{H_2O}}} \qquad [8.46]$$

Correspondingly, condensation can occur under super-saturated conditions on any hydrophilic surface:(210)

$$R_{\mathrm{w,g\rightarrow l}} = \sqrt{\frac{2 M_{\mathrm{H_2O}} RT}{\pi}} \alpha_{\mathrm{m}} a_{\mathrm{gl}} \left(c_{\mathrm{g,H_2O}} - c_{\mathrm{H_2O,sat}} \right) \qquad [8.47]$$

Here, α_{m} is the "mass accommodation coefficient" and is given a value of 0.04. The volumetric interfacial surface area was given as a_{gl} = 1000 m^{-1}.

Another approach encountered in some models is the use of log-law formulas:(113, 166)

$$R_{\mathrm{w}} \propto \mathrm{s_l} \ln\left(\frac{p_{\mathrm{A}} - p_{\mathrm{H_2O,sat}}}{p_{\mathrm{A}} - p_{\mathrm{H_2O}}}\right) \qquad [8.48]$$

9. TWO-PHASE MODELS OF THE MICROPOROUS LAYER (MPL)

9.1 GENERAL CONSIDERATIONS FOR TWO-PHASE TRANSPORT IN THE MICROPOROUS LAYER

The MPL and GDL regions of a PEMFC are broadly similar in terms of the relevant two-phase physics. Both regions are free from the ionomer phase, and are mixed wettability materials with net hydrophobicity. The MPL is differentiated principally by its much smaller mean pore size, which, given the hydrophobic nature of the material, discourages condensation. The small mean pore size also increases the importance of Knudsen diffusion to gas-phase reactant transport in the MPL. The presence of cracks in an MPL could significantly alter the appropriate two-phase properties to be used in this region, and lower the discrepancy between this region and the GDL.(35)

Weber and Newman promoted the description of the MPL as a separate, 'sandwiched', layer to be treated according to the same physical model as the bulk GDL, but with altered thermodynamic and transport properties.(214) Although they gave distinct values for the capillary pressure-saturation and permeability relations in the MPL, they did not consider any variation in the rate of evaporation-condensation.

In one recent study with a basis in experimental measurement, two-phase properties of the MPL were observed to have a weak effect on overall PEMFC response.(23)

9.2 GDL-MPL INTERFACE

The GDL-MPL interface is an instance of a boundary between two domains with different two-phase material properties. As noted in Section 4.1, continuity of pressure at such an interface requires a discontinuity of liquid water saturation.(27, 125) It has also been asserted, however, that the discontinuous pore structure at the GDL-MPL interface creates a "liquid-entry pressure" and hence a discontinuity in the liquid and capillary pressures.(215) No consistent theory has been offered for deriving this liquid-entry pressure, and it would seem surprising for its magnitude to be large compared to the liquid pressure drops through the adjacent porous media.

The most general approach, and one that is consistent with a negligible liquid pressure drop at the MPL interfaces, is to set the liquid water mass flux proportional to an interfacial pressure drop:(91)

$$\mathbf{N}_{\mathrm{w,GDL\rightarrow MPL}} = k_{\mathrm{int,GDL/MPL}}\left(p_{\mathrm{l,GDL}} - p_{\mathrm{l,MPL}}\right) \qquad [9.1]$$

As the interfacial rate constant $k_{\mathrm{int,GDL/MPL}}$ tends to larger values, continuity of pressure is approached. A value of $k_{\mathrm{int,GDL/MPL}} \approx 2 \times 10^{-4}$ kg m^{-2} s^{-1} Pa^{-1} has been reported to give near-continuous liquid-phase pressure.

Since the MPL-GDL interface may not be sharp, but may involve interpenetration of material, smoothed, continuous functions for porosity, permeability and contact angle have been suggested as superior to a sharp interface model.(216) It has been reported that neutron imaging shows no particular liquid saturation discontinuity across the MPL-GDL interface; however, the resolution of this technique at the interface may not be adequate.(40)

10. TWO-PHASE MODELS OF THE GAS CHANNEL

Two-phase flow in the open volume of the gas channels of a PEMFC occurs in regions with significantly larger length scales than the PEMFC porous media: the gas channel cross-sectional diameter is typically of order 1 mm compared to pore sizes ≤ 10 μm in the GDL. Consequently, the dynamics of two-phase flow in these regions may be quite different, and more difficult to describe in a volume-averaged manner.(217) Observed flow regimes range from "mist flow" (dispersed liquid droplets) to film flow in which liquid water coats the channel walls, and even slug flow, in which liquid water volumes may fully occupy the gas channel cross-section.(42, 218)

10.1 CONTINUUM TWO-PHASE MODELS OF THE GAS CHANNEL

Many researchers have emphasised the study of resolved liquid morphology as essential to explain droplet formation and transport in gas channels; it is beyond the scope of this review, which focuses principally on the description of the gas channel in terms of boundary conditions applied to a two-phase description of the GDL. In the following section we briefly review approaches to continuum models of two-phase transport in gas channels.

Meng et al. and Ye et al. have advocated a pseudo-two-phase "homogeneous mist flow" model of the gas channel in which saturation is resolved in the gas channel, but liquid water is supposed to be present as infinitesimal droplets, such that the apparent liquid water velocity in the gas channel matches the prevailing gas-phase velocity.(189) Wu et al. noted that the results of mist flow models closely approach those from the complete evaporation assumption.(19, 219) Anderson et al. suggested that mist flow is not in good agreement with *in situ* observations.(218) It has been argued that an abrupt transition to the mist state at the gas channel-GDL interface effectively ignores the influence of surface tension.(220)

Some models have simply assumed that liquid water in the free-flow channel obeys a Navier-Stokes or Darcy-Brinkman equation.(210, 221) Alternatively, models based on a shared pressure field, including the Euler-Euler equation, have also been explored.(90, 141) It has also been conventional to neglect evaporation-condensation phase change in the gas channel.(113, 222)

Coppo et al. define a variable ratio between liquid velocity and gas velocity in the gas channel as:(137)

$$\frac{\mathbf{u}_\mathrm{l}}{\mathbf{u}_\mathrm{g}} = 1 - 2\sqrt{\frac{2\sin\theta_\mathrm{c}}{\mathrm{We}\cdot C_\mathrm{D}}} \qquad [10.1]$$

where We is the Weber number and C_D is the drag coefficient between liquid droplets and the gas flow. The contact angle θ_c is expressed here for the GDL exterior surface. The velocity ratio in [10.1] was equated to a constant value of 0.05 by Abdollahzadeh et al.(223)

He et al. proposed a two-fluid model assuming equal gas- and liquid-phase pressures, incorporating drag and lift forces acting to transfer momentum between the gas and liquid flows:(224)

$$\mathbf{f}_{\mathrm{g,drag}} = -\mathbf{f}_{\mathrm{l,drag}} = 0.75 C_\mathrm{D} \frac{\rho_\mathrm{g}}{d_\mathrm{drop}} s_\mathrm{l} \left|\mathbf{u}_\mathrm{l} - \mathbf{u}_\mathrm{g}\right| \mathbf{u}_\mathrm{l} \qquad [10.2]$$

$$C_\mathrm{D} = \frac{24}{\mathrm{Re}_\mathrm{g}}\left(1 + 0.1925\,\mathrm{Re}_\mathrm{g}^{0.63}\right) \qquad [10.3]$$

$$\mathrm{Re}_\mathrm{g} = \left(1 - s_\mathrm{l}\right)\frac{\rho_\mathrm{g} d_\mathrm{drop}\left|\mathbf{u}_\mathrm{l} - \mathbf{u}_\mathrm{g}\right|}{\mu_\mathrm{g}} \qquad [10.4]$$

$$\mathbf{f}_{\mathrm{g,lift}} = -\mathbf{f}_{\mathrm{l,lift}} = 0.75 C_\mathrm{L} \rho_\mathrm{g} s_\mathrm{l} \nabla \mathbf{u}_\mathrm{g}\left(\mathbf{u}_\mathrm{l} - \mathbf{u}_\mathrm{g}\right) \qquad [10.5]$$

$$C_{\mathrm{L}} = C_{\mathrm{L,ref}} \left(1 - 2.78\left(s_{\mathrm{l}} - 0.2\right)\right) \quad [10.6]$$

The latter model was subsequently adapted to an M^2 model treatment of the mixed gas-liquid flow in the gas channel.(225)

An apparent drag coefficient for two-phase flow in gas channels has alternatively been proposed based on the *Ishii-Zuber equation*:(156, 160, 226)

$$C_{\mathrm{D}} = \frac{24}{\mathrm{Re}}\left(1 + 0.1\,\mathrm{Re}^{0.75}\right) \quad [10.7]$$

where Re is the Reynolds number of the external flow (77).

10.2 LIQUID WATER TRANSPORT AT THE GAS CHANNEL-GDL INTERFACE

In 2014, Weber et al. described the treatment of the boundary condition for liquid water transport at the gas channel-GDL interface as a significant contemporary challenge for the development of PEMFC models (40); this boundary condition ultimately controls the overall water content in the GDL, CL and membrane regions. Definitions such as zero saturation at a GDL outlet (155) either imply infinitely fast evaporation, or else force all evaporation to take place further upstream; therefore, liquid water pressure or capillary pressure outlet conditions are recommended.(40) Models solving full two-phase flow for the gas channel may enforce a saturation discontinuity between the gas channel and GDL by defining equality of both gas and liquid phase pressures at the boundary.(227)

He et al. proposed zero liquid water content at the gas inlet to the GDL in an interdigitated flow field design, and zero saturation gradient at the GDL outlet.(207) A number of other authors (see accompanying literature review spreadsheet) have imposed a fixed saturation at the GDL-gas channel boundary, including as an empirical variable linked to cell voltage (189). Liu et al. suggested zero liquid water flow through the interface (228), which seems implausible as it forces evaporation upstream; in combination with evaporation-condensation equilibrium, the zero liquid water flow condition appears (unsurprisingly) to require specific control of numerical settings at the boundary in order to be solvable.(229) Cao et al. define the saturation gradient as zero normal to the interface, such that capillary action falls to zero at the interface (230) – this also seems to lack a clear physical justification.

Berning et al. treated the interface as a thin layer with a distinct liquid water permeability, arguing that drainage occurs from the GDL to the gas channel across only a finite active area A_{act}.(141) By specifying the droplet size at detachment, an effective permeability of the gas channel-GDL interface is given as:

$$\kappa_{\mathrm{eff,int}} = \frac{d_{\mathrm{drop}}^2}{2}\frac{A_{\mathrm{act}}}{A_{\mathrm{cell}}} \quad [10.8]$$

and the corresponding boundary condition is:

$$\mathbf{N}_{\mathrm{w}} \cdot \mathbf{n} = -\frac{\rho_{\mathrm{w}}\kappa_{\mathrm{eff,int}}}{\mu}\nabla p \cdot \mathbf{n} \quad [10.9]$$

This expression was extended to apply a pressure-proportional flux under conditions of capillary pressure exceeding breakthrough pressure p_{BT}, and a zero pressure condition otherwise:(178)

$$\mathbf{N}_{\mathrm{w}} \cdot \mathbf{n} = k_{\mathrm{int}}\ \mathrm{step}\left(\frac{p_{\mathrm{l,GDL}} - p_{\mathrm{l,channel}}}{\Delta p_{\mathrm{smooth}}}\right)\left(p_{\mathrm{l}} > p_{\mathrm{BT}}\right) \quad [10.10]$$

where step(x) is a smoothed step function transitioning from 0 for negative input to 1 for positive input. An interfacial rate constant $k_{\mathrm{int}} = 10^{-6}$ kg m^{-2} s^{-1} was assumed.

Outflow velocity has also been defined directly in terms of the channel velocity:(113)

$$N_{\mathrm{w,int}} = k_{\mathrm{w,int}} \varepsilon_{\mathrm{GDL}} s_{\mathrm{l}} \max\left(p_{\mathrm{cap}} + \frac{1}{2} \rho_{\mathrm{l}} \mathbf{u}_{\mathrm{l}}^2, 0 \right) \quad [10.11]$$

10.3 DETAILED DROPLET DETACHMENT MODELS

Many more detailed theories for the liquid water transport process at the gas channel-GDL interface have focused on the dynamics of liquid water droplet instability and detachment at the downstream face of the GDL, as discussed in a recent review.(231) This process is facilitated by wicking from hydrophobic sites, which are typically assumed to be present at the interface (108); at hydrophilic sites, a drag force from the air flow would be required to detach liquid water, which will otherwise wet the exterior surface of the GDL.(42, 218) The droplet diameter at which detachment takes place depends on the balance of drag and adhesion forces, which are difficult to determine experimentally (40); a simplified theoretical model has been proposed (224). Non-uniform (localised) droplet formation at the gas channel-GDL interface creates regions of blocking with respect to reactant transport; simulations to investigate these more closely depend on phase-resolved methods such as volume-of-fluid calculations (232), which are beyond the scope of this review.

Adhesion theory is based on evaluating a balance between adhesion force and one or more of the forces that drive the droplet away from the interface (pressure force, shear force, gravity).(149) Considering gravity alone leads to "Tate's law", but gravitational forces will be negligible for small droplet sizes (as distinct from slug flows, see also "Dimensional analysis" above). For highly laminar (Stokes) flow, shear forces grow linearly with droplet size, i.e. at the same rate as surface tensile forces, but any corrections to Stokes flow for larger droplets may lead to the surface tensile force being overcome.

Gurau et al. have described a specific adhesion model termed "eruptive water ejection".(24, 156, 160) According to this theory, a defined surface number density of droplets is present at the GDL-gas channel interface. These droplets are given a spherical cap geometry and so expand with a linearly increasing total force of surface tension with radius, until detachment occurs as the surface tensile force is overcome by gravity or shear forces; the detachment of droplets into the GDL is interpreted as rate-limiting with respect to overall moisture transport, and so controls the degree of saturation in the GDL. One plausible extension of this model (not yet present in the literature) could be accomplished by expressing a cyclic time average of the eruptive water ejection in order to quantify the general water transfer rate from GDL to gas channel.

10.4 EFFECTIVE MEDIA APPROXIMATIONS OF THE GAS CHANNEL

Several authors have suggested effective media approximations to describe liquid water transport in gas channels, by representing the combined solid and void space of the gas channels as a homogenised pressure medium, and then expressing the flow based on two-phase Darcy's law.(224, 233-235) As the gas channel diameter is much larger than the GDL pore sizes, the Darcy's law approximation (discussed above under "Two-phase Darcy's law") is much weaker – such models are not capable of reproducing the subtlety of flow regimes observed experimentally.(141, 236) However, they may still prove accurate under certain operating conditions.

Wang et al. used the M^2 model to describe a homogenised "gas channel" medium, in combination with a standard Leverett function using a hydrophilic contact angle ($\theta_{\mathrm{c,gc}} = 80°$); flow channel geometry is described using heterogeneous and anisotropic permeability, with quartic dependence on liquid water saturation ($n_\kappa = 4$).(234) A subsequent full cell development of this model used $\theta_{\mathrm{c,gc}} = 60°$ and $n_\kappa = 5$ (237); the latter parameterisation has also been used in a similarly formulated two-fluid model, in which it is recognised that the drag forces due to air flow are significantly more important than capillary-driven transport, under normal conditions.(235) Rizvandi et al. gave a constant capillary diffusion coefficient $D_{\mathrm{cap}} = 10^{-3}$ m^2 s^{-1} in the gas channel (114), which is one or two orders of magnitude lower than suggested by the Leverett equation.

11. TWO-PHASE MODELS OF THE CATALYST LAYER (CL)

11.1 GENERAL CONSIDERATIONS FOR TWO-PHASE TRANSPORT IN THE CATALYST LAYER

Thin liquid water films (implying 'flooding' of the catalyst layer) arise on ionomer-Pt/C agglomerates even at very low liquid water saturation.(37) Given that transport of reactants (H_2 in the anode CL, O_2 in the cathode CL) is orders of magnitude slower in condensed phases than in the gas-phase, blocking of the gas-phase transport paths by flooding is a major contributor to transport limitations on PEMFC performance. Modelling methods for the catalyst layer (excluding two-phase phenomena) have been discussed more widely in a prior review.(3)

Compared to the GDL and even MPL, the catalyst layer (CL) exhibits significant heterogeneity and a broad pore-size distribution.(177) Generally, there is even less reason than for the GDL to expect that standard porous media theory is appropriate from a predictive point-of-view, given the presence of the additional ionomer phase in the CL and the occurrence of a volume-averaged material source/sink due to electrocatalytic reactions.(159)

The catalyst layer is typically sufficiently thin for through-layer pressure differences to be negligible, even in the liquid phase.(179) Consequently, it has often been assumed that that the CL does not need to be resolved spatially.(3, 6) Where a volumetric resolution of the CL is attempted in models, difficulty arises because the CL is challenging to access experimentally due to its small dimensional extent; consequently, the measured data for two-phase thermodynamic and transport properties of the CL have limited scope. Measurements of properties such as external contact angle (238) are inconclusive in terms of the information they provide for liquid water transport modelling. Soboleva et al. have presented sorption curves for CL materials, but even with comparison to Nafion blanks as a reference, it is challenging to disentangle ionomer sorption phenomena from capillary uptake of liquid water in structural pores.(239) The determination of two-phase thermodynamic properties of partially saturated porous media (i.e. capillary pressure-saturation relation) in the presence of sorption is still an unsolved issue in the field.

The CL is a site where a careful balance of water content is needed to maintain high proton conductivity in ionomer material, but to avoid flooding. The optimal ionomer content of the CL can be tuned to the relative humidity of operation, and needs to consider the distinct pore size distributions of CLs prepared from different carbon material types.(239) Rate limitation to evaporation-condensation processes is likely to create perceptible performance losses.(240) The small pore size in the CL may contribute to more rapid rates of evaporation than are achievable in the GDL, in spite of the difference in hydrophobicity; it has been suggested that, for some temperatures and pore size distributions, evaporation in the cathode CL can keep pace with the rate of generation of water in the ORR.(241)

11.2 TWO-FLUID MODELS OF THE CATALYST LAYER

11.2.1 Interface thermodynamics

A suitable isotherm for apparent vapour pressure in the CL has been defined as follows, based on the Kelvin equation [7.1] and a locally constant enthalpy change of vaporisation (ΔH_{vap}):

$$p_{vap,app} = p_{vap,0,CL} \exp\left(\frac{-\Delta H_{vap}}{RT}\right)\exp\left(p_{cap,CL}\frac{M_{H_2O}}{RT\rho_w}\right) \quad [11.1]$$

with reported values $p_{vap,0,CL} = 1.18 \times 10^6$ atm, $\Delta H_{vap} \approx 43$ kJ mol^{-1}.(241)

In some models (see accompanying literature review spreadsheet), the capillary pressure-saturation relation has been given assuming a Leverett function. However, there is even less likelihood of this function being physically representative than is the case for the ionomer-free porous diffusion

media.(65) Alternatively, capillary pressure-saturation relations may be derived from the pore-size distribution, as discussed in the following section.

11.2.2 Pore-size distribution analysis

A number of models of the CL use a bimodal pore-size distribution to consider separate wetting of micropores (primary pores, $r < 10$ nm) and macropores (secondary pores, $r \geq 10$ nm).(30, 159, 241) The assumption of pore filling up to a critical radius (see "Pore-size distribution analysis: capillary pressure and saturation" above) allows the saturation to be defined as follows:(241)

$$s_{\mathrm{L}} = \frac{1}{\varepsilon_{\mathrm{CL,dry}}} \int_0^{r_{\mathrm{crit}}} \frac{d\varepsilon_{\mathrm{CL}}(r')}{dr'} dr' \qquad [11.2]$$

Subsequent analysis of the bimodal pore-size distribution function suggests that typical CL composites are hydrophilic for $s_{\mathrm{l}} < 0.7$ and hydrophobic for $s_{\mathrm{l}} > 0.7$, due to the different wettabilities of different pore sizes.(159)

Strahl et al. used the pore-size distribution model while assuming a thin concentric liquid water layer within spherical pores, where ionomer is contained only within secondary pores.(30) Liquid is then assumed to fill the central air pore up to a critical radius given by [7.33]. The liquid water volume in primary pores is then given as the proportion of the total pore size not occupied either by air or by Pt particles. Assuming that the Pt particle volume is negligible and taking a fixed primary pore size r_{pp} (set as 10 nm) gives the primary pore saturation as:

$$s_{\mathrm{l,p}} = 1 - \left(\frac{r_{\mathrm{crit}}}{r_{\mathrm{pp}}} \right)^3 \qquad [11.3]$$

Combining [7.33] and [11.3] gives a capillary pressure-saturation relation for the CL with only primary pores partially saturated as: (30)

$$p_{\mathrm{cap}} = \frac{2\gamma \cos\theta_{\mathrm{c,CL}}}{r_{\mathrm{pp}} \left(1 - s_{\mathrm{l,p}}\right)^{\frac{1}{3}}} \qquad [11.4]$$

On the basis of a small ionomer sorption characteristic, a similar formula was assumed to apply for secondary pores, using a secondary pore radius r_{sp} to extend [11.4] to s_{l} values where primary pores are fully saturated.

The Strahl primary pore size distribution model gives the volumetric electroactive area as a function of the volume density of Pt particles $n_{\mathrm{vol,Pt}}$ and a vaguely specified curvature length scale h_{s}:(30)

$$a_{\mathrm{CL}} = n_{\mathrm{vol,Pt}} 2\pi r_{\mathrm{Pt}} \max\left(h_{\mathrm{s}} + r_{\mathrm{pp}} \left(1 - s_{\mathrm{l,p}}\right)^{\frac{1}{3}}, 2r_{\mathrm{Pt}} \right) \qquad [11.5]$$

11.2.3 Gas-phase tortuosity

Wang et al. collated experimental measurements of gas-phase tortuosity in the CL, and proposed the following expression:

$$\frac{D_{\mathrm{eff,MPL}}}{D} = \varepsilon^{m_D} \left(1 - s_{\mathrm{l}}\right)^{n_D} \qquad [11.6]$$

where if Knudsen diffusion is excluded, $m_D = n_D = 4$, but if Knudsen diffusion is incorporated in the theoretical model, $m_D = n_D = 5.5$.(33) The degree of saturation will influence the distribution of gas-accessible pore sizes, and hence the transition between Knudsen diffusion of reacting gases and normal continuum diffusion.

11.2.4 Evaporation-condensation rate

Eikerling et al. proposed that the evaporation rate can be determined in a manner analogous to the He equations for the GDL, but proposing that the capillary radius can be used to yield the gas-liquid interfacial volumetric surface area directly:(241)

$$R_{\mathrm{w,l\rightarrow g,CL}} = k_{\mathrm{v}} \frac{d_{\mathrm{CL}} \varepsilon_{\mathrm{CL,dry}}}{2r_{\mathrm{cap}}} \left(p_{\mathrm{vap}} - p_{\mathrm{H_2O}} \right) \quad [11.7]$$

where d_{CL} is catalyst layer thickness.

11.3 SORPTION IN TWO-PHASE MODELS

Within the CL, the sorption equilibrium of water into the ionomer must be considered in addition to the evaporation-condensation equilibrium. Sorption of water into the membrane under both liquid- or gas-equilibrated conditions has been discussed previously.(1) Weber et al. assumed an equivalent chemical potential between water vapour and water in the membrane phase, at the catalyst layer-membrane interface.(6) Olapade et al. suggested that for systems at RH < 100%, the water sink from sorption is sourced entirely from the vapour phase; at higher RH, the water source from each phase is scaled according to the saturation.(163)

Wu et al. have addressed the need for care over the consistency of thermodynamic equilibrium statements between three phases (when sorption into the membrane is considered), as these may become inconsistent with the chosen boundary conditions at the interfaces between different regions of the PEMFC.(219) Correspondingly, Siegel et al. described the three-phase near-equilibrium in the catalyst layer between dissolved water (in membrane phase), liquid and gas-phase water through a series of linear kinetic phase change relations with sufficiently high rate constants to maintain equilibrium to good approximation.(242)

The sorption properties of nanoscale ionomer structures in the CL are reported to differ from the bulk ionomer, with lower water uptake noted (177); some authors have assumed a constant water "effectiveness factor" which is a ratio between the water content of the CL ionomer and that of bulk ionomer for like activity, and typically is given values between 0.3 and 0.5.(243, 244) Such a treatment necessarily creates uncertainty – which is not yet resolved in the academic community – as to whether the membrane water content or water activity should be assumed to be the continuous variable at a discretely resolved CL-membrane interface.(40)

The presence of ionomer may influence the pore volume of the CL, due to swelling of the ionomer phase under water sorption. A linear relation of membrane volume fraction to membrane water content has been proposed:(209)

$$\varepsilon_{\mathrm{mem}} = \varepsilon_{\mathrm{mem,0}} + 0.0126\lambda \quad [11.8]$$

11.4 IN WHAT PHASE IS WATER GENERATED AT THE CATHODE?

In two-phase models in which the volume fractions of liquid- and gas-phase water are computed independently, it is typically necessary to consider the phase in which water produced by the oxygen reduction reaction is generated within the cathode CL. Additionally, electroosmotic drag phenomena may cause a water sink accompanying the hydrogen oxidation reaction in the anode CL. Where ionomer water content is also solved self-consistently with membrane sorption, the water source may be applied to the ionomer phase, also. The settings used in various two-phase flow models are summarised in the accompanying literature review spreadsheet.

The most common choice of phase for product water from the ORR is the liquid phase, and the definition of product water in the gas phase has been specifically criticised by Wu et al.(245) For models in which thermodynamic equilibrium between the liquid and gas phases is assumed, such as

the M^2 model, the definition of the water product phase has no impact, although the energetics of the ORR must still be described self-consistently. Models focusing only on the GDL, and so treating the CL as an idealised water source, may choose to avoid the question entirely.(87) In the case of the Weber-Newman model, equality of liquid pressure is enforced across the thin CL, represented as a boundary between the GDL and membrane; therefore, the ORR product water may arise in practice in either phase or be sorbed into the membrane, depending on the prevailing pressure and temperature conditions.(6)

Shah et al. scale the source term depending on the local degree of saturation: water is sourced to the gas phase if the partial pressure of water vapour is below the vapour pressure, but otherwise, water is sourced to the liquid phase.(209) A similar approach has also been used to assume that ORR product water is absorbed into the ionomer from different phases in the CL, depending on the local water activity.(246) In this case, sorption acts to/from the liquid phase for saturations above a "critical saturation" set equal to the immobile saturation of the composite material.

11.5 INFLUENCE OF LIQUID WATER SATURATION ON CATALYTIC TURNOVER

The most common, simple approach to account for the role of liquid water on catalyst layer flooding is to assume that catalytic activity scales polynomially with the gas-phase volume fraction in the pores. That is, an effective reference current density is used in the kinetic model where:

$$i_{\mathrm{ref}} = i_{\mathrm{ref},0}\left(1 - s_{\mathrm{l}}\right)^{n_{\mathrm{CL}}} \qquad [11.9]$$

in which $i_{\mathrm{ref},0}$ is the reference current density under dry conditions. The trend is most often assumed to be linear ($n_{\mathrm{CL}} = 1$), but experiment has suggested values between $0.5 \leq n_{\mathrm{CL}} \leq 0.62$, depending on the measurement technique used to infer this value.(84)

This type of empirical treatment implicitly neglects any specific, mechanistic role for liquid water in the CL, although both H_2 and O_2 reactants are soluble in liquid water, and it is an acceptable proton conductor in which both the HOR and ORR are known to be catalysed at Pt surfaces (247). Moreover, the distribution of water at the active surface may be significantly non-uniform compared to the average degree of saturation in the CL.(121) Wu et al. consider, and discount, the possibility of an electrocatalytic reaction at the Pt-H_2O(l) interface, in the absence of ionomer (219), although such reactions are certainly known macroscopically (247). Some works have proposed full flooding of the CL pores with liquid water.(248, 249)

The principal alternative to a polynomial scaling is the use of the spherical flooded agglomerate model, whose basis and justification, along with some criticisms, are summarised elsewhere.(3) In this type of agglomerate model, a thin water layer of defined thickness is assumed to exist as a concentric spherical shell surrounding each ionomer-Pt/C agglomerate particle (i.e., water is filling secondary pores in the CL structure); some authors consider the combination of an agglomerate model with two-phase transport in the CL to be essential to reproduce experimental data accurately (250, 251).
By assuming that all of the liquid water present in the CL occurs as such a film, the film thickness becomes a dependent function of the local, average saturation and the agglomerate particle properties. The H_2 and O_2 reactants must then dissolve in and diffuse through this film to reach a reaction site, introducing a saturation-dependent transport limitation. The solubility of the gases in the water film may differ from that in the membrane.(1, 3, 103)

Values for O_2 diffusivity in liquid water close to $D_{\mathrm{O2,w}} = 5 \times 10^{-9}$ m^2 s^{-1} have generally been reported.(65) Xing et al. give:(252)

$$D_{\mathrm{O_2,w}} \,/\, \mathrm{m^2\ s^{-1}} = 7.4 \times 10^{-8} T \frac{\sqrt{2.6 M_{\mathrm{H_2O}} \,/\, 1\ \mathrm{kg\ mol^{-1}}}}{\mu_{\mathrm{w}} \left(V_{\mathrm{m,O_2}} \,/\, 1\ \mathrm{m^3}\right)^{0.6}} \qquad [11.10]$$

In models from the Nguyen group, originating with Lin et al. (193), a cylindrical agglomerate model is combined with a liquid water film. This model assumes that the ionomer phase is water-saturated. The film thickness is expressed assuming a thin (quasi-planar) liquid water layer, in terms of saturation, dry porosity of the CL excluding ionomer, and the volumetric surface area of the agglomerate particles:

$$d_{\mathrm{w}} = \frac{s_{\mathrm{l}}\varepsilon_{\mathrm{CL,dry}}}{a_{\mathrm{agg}}} \qquad [11.11]$$

The same thin-film approach has been applied subsequently in combination with an experimentally measured capillary pressure-saturation relation for the CL (17), and has been applied to the spherical geometry also (19, 250).

A rigorous combination of the agglomerate model with a two-phase CL model was introduced for the spherical agglomerate geometry by the Shah group.(209) This approach has been followed subsequently by several authors (see accompanying literature review spreadsheet). The water film thickness is expressed as a function of the agglomerate properties as:

$$d_{\mathrm{w}} = \left(r_{\mathrm{agg}} + d_{\mathrm{film}}\right)\left(\left(1+\frac{3s_{\mathrm{l}}\varepsilon_{\mathrm{CL,dry}}}{4\pi N_{\mathrm{agg}}\left(r_{\mathrm{agg}}+d_{\mathrm{film}}\right)^{3}}\right)^{\frac{1}{3}} - 1\right) \qquad [11.12]$$

This formula contained an error in the second term in the original publication (209), which was corrected subsequently (103). N_{agg} represents the number of agglomerates per unit dry material volume. Writing

$$N_{\mathrm{agg}} = \frac{\varepsilon_{\mathrm{Pt/C}}}{\frac{4\pi}{3}r_{\mathrm{agg}}^{3}\left(1\text{-}\varepsilon_{\mathrm{CL,dry}}\right)} \qquad [11.13]$$

yields a corresponding expression for film thickness as:(252)

$$d_{\mathrm{w}} = \left(r_{\mathrm{agg}} + d_{\mathrm{film}}\right)\left(\left(1+\frac{s_{\mathrm{l}}\varepsilon_{\mathrm{CL,dry}}\left(1-\varepsilon_{\mathrm{CL,dry}}\right)}{\varepsilon_{\mathrm{Pt/C}}}\left(\frac{r_{\mathrm{agg}}}{r_{\mathrm{agg}}+d_{\mathrm{film}}}\right)^{3}\right)^{\frac{1}{3}} - 1\right) \qquad [11.14]$$

A different expression has been given by Jo et al.(132), but the latter is either simply in error, or else the assumptions or definitions leading to its derivation are not clearly expressed. In the thin film limit, using linear rather than spherical diffusion (i.e. assuming a quasi-planar thin film), Schwarz et al. wrote more simply:(65)

$$d_{\mathrm{w}} = \frac{\varepsilon_{\mathrm{CL,dry}}s_{\mathrm{l}}}{\varepsilon_{\mathrm{mem}}}d_{\mathrm{film}} \qquad [11.15]$$

The parameterisation and parameter sensitivity of two-phase agglomerate models has been studied extensively by Li et al.(253)

Alternatively, water film transport resistance has been approximated directly as:(254)

$$\mathbf{N}_{\mathrm{O_2}} = \frac{k_{\mathrm{diff,film}}}{s_{\mathrm{l}}^{\frac{1}{3}}}\Delta c_{\mathrm{O_2}} \qquad [11.16]$$

with $k_{\mathrm{diff,film}}$ = 0.01 m s^{-1}.

11.6 MPL-CL INTERFACE

Imperfect contact at the MPL-CL interface was considered by Swamy et al.(255) This work identified three characteristic roughness length scales, measured by optical profilometry *ex situ* on MPL and CL samples. Based on a rough surface contact model, it was concluded that in regions under the channel, the MPL-CL interface can store up to 3 mg cm^{-2} of liquid water, while under the land, the compression contact pressure is high enough to prevent this. It has been suggested that these interfacial voids at the MPL-CL interface can act as locally saturated blocking sites to moisture transport; in a macro-homogeneous model, this effect might be included as a lumped transport resistance at the interface.(256)

12. CONCLUSION

This report has collated methods for the theoretical description of the influence of liquid water in PEMFC operation. Principally, researchers developing 1D to 3D models of PEMFCs describe the porous media (GDL, MPL, CL) as homogenised, using models such as the two-fluid model to represent two-phase flow. These models depend upon effective transport properties which are frequently derived from capillary pressure-saturation relations and water-air contact angles; often, these source data (e.g. Leverett functions) are drawn from origins of little relevance to the specific materials present in the PEMFC. Increased efforts towards characterisation of PEMFC porous materials (principally *ex situ*) has made available some additional empirical data, which is not always compatible with simplified theoretical models; use of such data is expected to be an increasingly important aspect in future PEMFC models.

Throughout the literature, the complexity of the various two-phase models leads to a lack of clarity in reporting, and difficulty in reproduction of theoretical results. Often, the meaning of terms in equations is absent or vague in the literature; equally, some errors persist and have been copied. This document has attempted to identify common or unifying approaches across multiple authors, remarking on trends of popularity and scope for parameterisation, while highlighting persistent errors. An additional, major challenge is that different models may fit certain experimental data sets equally well, subject to different parameterisation.

The following significant open scientific questions remain as subjects for future study:

- What are the bounds on reliability of the various models and parameterisations discussed?
- Can *in situ* / *operando* measurements firmly exclude as inappropriate certain modelling approaches?
- How can empirically measured properties of the PEMFC porous media be most effectively parameterised?
- Do the electrocatalytic reactions ever require a momentum source term in the two-phase flow equations? (Section 5.3)
- Can a “pseudo-phase equilibrium approach” for handling sharp interface problems be derived in a physically motivated manner, improving on prior work? (Section 8.4)
- What is the most appropriate way to set liquid water boundary conditions at the GDL-gas channel interface, perhaps considering also the mechanism of droplet detachment? (Sections 10.2 and 10.3)
- How can the three-phase thermodynamic equilibrium between gas, liquid and ionomer phases for the water component in the CL be handled consistently? (Section 11.3)

TABLE OF ABBREVIATIONS

CL	catalyst layer
GDL	gas diffusion layer
HT	high temperature

MPL	microporous layer
ORR	oxygen reduction reaction
PEMFC	polymer electrolyte membrane fuel cell
PTFE	polytetrafluoroethylene
PVDF	polyvinylidene fluoride
RH	relative humidity

TABLE OF SUBSCRIPTS

act	active
agg	agglomerate
ave	average
cap	capillary
comp	compressed / compression
crit	critical
diff	diffusional
dry	in dry condition ($s_l = 0$)
eff	effective
eq	equilibrium
g	gas (phase)
h+	hydrophilic
h-	hydrophobic
l	liquid (water) (phase)
lim	limiting
max	maximum
mol	molar
pp	primary pore
ref	reference state
res	residual
sat	saturated
sol	solutal
sp	secondary pore
vap	(water) vapour / vaporisation
w	water
$\parallel$	in-plane
$\perp$	through-plane

TABLE OF SYMBOLS

Symbol	Unit	Definition
A	1	Empirical coefficient, Natarajan capillary pressure model
a_i	1	Empirical coefficients, X.D. Wang capillary pressure model
a_i	1	Empirical coefficients, Rizvandi planar transport model
a_i	1	Empirical coefficients, X.D. Wang capillary pressure model
A_{act}	m^2	Active drainage area from GDL to gas channel
a_{agg}	m^{-1}	Interfacial surface area at surface of agglomerate particles, per unit composite volume
a_{CL}	m^{-1}	Electroactive area of CL per unit composite volume
A_{cell}	m^2	Macroscopic cell (electrode) area
a_{LMi}	1	Empirical coefficients, LaManna Leverett function
a_N	1	Empirical coefficient, Natarajan capillary pressure model
a_{vol}	m^{-1}	Liquid-gas interfacial surface area per unit composite volume
a_{Yi}	1	Empirical coefficients, Ye capillary pressure model

a_γ	1	Empirical coefficient, Ziegler surface tension model
B	1	Empirical coefficient, Natarajan capillary pressure model
B_m	1	Spalding number
b_i	1	Empirical coefficients, X.D. Wang capillary pressure model
b_N	1	Empirical coefficient, Natarajan capillary pressure model
b_Y	Pa	Empirical coefficient, Ye capillary pressure model
C	1	Empirical coefficient, Natarajan capillary pressure model
C	mol m^{-3}	Component-averaged concentration (M^2 model)
C_D	1	Drag coefficient
C_L	1	Lift coefficient
$c_{w,k}$	mol m^{-3}	Concentration of water in phase k per total composite volume
c_Y	1	Empirical coefficient, Ye capillary pressure model
D	m	Empirical coefficient, Natarajan capillary pressure model
D_i	m^2 s^{-1}	Diffusion coefficient, species i in bulk gas
$D_{i,\mathrm{eff},k}$	m^2 s^{-1}	Effective diffusion coefficient, species i in region k
d_{drop}	m	Liquid water droplet diameter
d_{GDL}	m	GDL thickness
d_Y	Pa	Empirical coefficient, Ye capillary pressure model
D_{cap}	m^2 s^{-1}	Capillary diffusion coefficient (defined in Richards' equation)
$D_{\mathrm{eff},i}$	m^2 s^{-1}	Effective (macroscopic) diffusion coefficient of species i
d_{film}	m	Ionomer film thickness on CL agglomerates
$D_{\mathrm{sol},i}$	m^2 s^{-1}	Solutal diffusion coefficient of species i (M^2 model)
D_T	m^2 s^{-1} K^{-1}	Thermal diffusion coefficient
d_w	m	Water film thickness on CL agglomerates
Da	1	Damköhler number (ratio of water production rate to water diffusion rate)
E_a	J mol^{-1}	Activation energy
F	C mol^{-1}	Faraday constant
$\mathbf{f}_{k,\mathrm{drag}}$	N m^{-3}	Volumetric drag force acting on phase k
$\mathbf{f}_{k,\mathrm{lift}}$	N m^{-3}	Volumetric lift force acting on phase k
f_A	1	Area fractal dimension, Wu tortuosity model
$f_{r,k}$	1	Weighting constant, Weber pore-size distribution model
f_s	1	Shear interaction coefficient, two-fluid model
f_{vap}	1	Saturation-dependent coefficient, Langmuir evaporation rate formula
f_w	1	Saturated proportion of the reactant flow path, pseudo-two-phase models
f_τ	1	Tortuosity fractal dimension, Wu tortuosity model
$\mathbf{g}$	m s^{-2}	Gravitational acceleration
ΔH_{vap}	J mol^{-1}	Enthalpy change of vaporisation
h_s	m	Empirical coefficient, Strahl catalyst layer model
i_{cell}	A	Cell current density
$\mathbf{I}$	A m^{-2}	Total current density (M^2 model)
i_{ref}	A m^{-2}	Reference current density, electrode kinetics
J	1	Leverett function
J_K	1	Leverett function using data from Kumbur et al.
J_{LM}	1	Leverett function using data from LaManna et al.
J_{vG}	1	Leverett function equivalent to van Genuchten equation
$\mathbf{j}_k$	kg m^{-2} s^{-1}	Diffusive mass flux of phase k (M^2 model)
k_{int}	kg m^{-2} s^{-1} Pa^{-1}	Interfacial transport coefficient
k_c	s^{-1}	Condensation rate constant
k_v	Pa^{-1} s^{-1}	Evaporation rate constant
M_i	kg mol^{-1}	Molar mass, species i
M_{vap}	kg mol^{-1}	Mean molar mass of gas phase
m_{BC}	1	Empirical coefficient, Brooks-Corey equation

m_D	1	Tortuosity model exponent
m_{vG}	1	Empirical coefficient, van Genuchten equation
n	1	Unit vector, through-plane
n	1	Number of component species, M^2 model
N_{agg}	m^{-3}	Number density of agglomerates, per unit composite volume
n_{CL}	1	Electrode kinetics saturation-dependence exponent
n_D	1	Pore blockage exponent
n_{eq}	1	Empirical coefficient, Hsuen pseudo-phase-equilibrium model
n_{vGm}	1	Empirical coefficient, van Genuchten equation
n_κ	1	Permeability-saturation relation exponent
$\mathbf{N}_k$	kg m^{-2} s^{-1}	Effective mass flux of phase k
$\mathbf{N}_w$	kg m^{-2} s^{-1}	Effective mass flux of water (per unit composite cross-section)
n_κ	1	Exponent for permeability-saturation relation
p_{bc}	1	Correlation probability, Pasaogullari anisotropic tortuosity model
p_{BT}	Pa	Breakthrough pressure, Berning gas channel-GDL interface model
p_{cap}	Pa	"Capillary pressure", standardised = p_g-p_l
p_{comp}	Pa	GDL compression pressure
p_g	Pa	Absolute pressure in gas phase
p_l	Pa	Absolute pressure in liquid phase
p_{ref}	Pa	Reference pressure
p_{vap}	Pa	Vapour pressure (H_2O)
R	J K^{-1} mol^{-1}	Gas constant
R_k	1	Roughness factor of composite component k, Wood mixed wettability contact angle model
R	m	Pore radius
$r_{0,k}$	m	Mean pore radius, pore type k in pore-size distribution
r_{crit}	m	Critical maximum/minimum radius of saturation
r_{agg}	m	Agglomerate particle radius
r_{Pt}	m	Pt particle radius
R_w	kg m^{-3} s^{-1}	Mass source of water (per unit composite volume)
Re	1	Reynolds number
s_l	1	Liquid water saturation as fraction of porous media void space
$s_{l,eff}$	1	Effective liquid water saturation as fraction of porous media void space
$s_{l,res}$	1	Residual liquid water saturation as fraction of porous media void space
Sc_i	1	Schmidt number for diffusion of component i
Sh	1	Sherwood number
T	K	Temperature
T_0	K	Reference temperature
T	s	Time
$\mathbf{t}_i$	1	Unit vectors, in-plane
U	m s^{-1}	Component-averaged velocity (M^2 model)
$\mathbf{u}_k$	m s^{-1}	Effective (Darcy) velocity, phase k
V	1	Normalised pore volume, probability density function against pore radius
v_γ	1	Empirical coefficient, Ziegler surface tension model
w_i	1	Component-averaged mass fraction, species i (M^2 model)
$w_{i,k}$	1	Mass fraction, species i in phase k
w_{H2O}	1	Total water mass fraction
w_{PTFE}	%	wt% PTFE in material
We	1	Weber number
x_k	1	Mole fraction of component in phase k (M^2 model)
$x_{h\pm}$	1	Fraction of hydrophilic/hydrophobic pores in mixed wettability composite
A	1	Electroosmotic drag coefficient
α_{cap}	1	Empirical coefficient, Gurau capillary pressure model

α_m	1	Mass accommodation coefficient, evaporation rate
Γ	N m^{-1}	Surface tension of liquid-gas interface
γ_0	N m^{-1}	Surface tension of liquid-gas interface at reference temperature
γ_1	N m^{-1} K^{-1}	Surface tension of liquid-gas interface, temperature coefficient
γ_i	1	Advective coefficient of component species *i* (M^2 model)
γ_{vG}	1	Empirical coefficient, van Genuchten permeability equation
γ_ρ	1	Gravitational coefficient (M^2 model)
δ_{eq}	1	Empirical coefficient, Hsuen pseudo-phase-equilibrium model
E	1	Total void fraction (M^2 model)
ε_k	1	Volume fraction of component *k*
ε_{lim}	1	Residual (limiting) gas-phase volume fraction
θ_c	1	Contact angle of liquid-gas interface at a solid surface (defined as interior angle to liquid phase)
η_M	1	Empirical coefficient, Mualem functions
K	m^2	Component-averaged permeability (M^2 model)
κ_0	m^2	Dry permeability of the porous medium ($s_l = 0$)
κ_k	m^2	Permeability, phase *k*
λ_k	1	Relative mobility of phase *k* (M^2 model)
λ_{PSD}	1	Interconnectivity parameter, pore-size distribution
M	Pa s	Component-averaged dynamic viscosity (M^2 model)
μ_k	Pa s	Dynamic viscosity of phase *k*
P	kg m^{-3}	Component-averaged density (M^2 model)
ρ_k	kg m^{-3}	Density of phase *k*
ρ_w	kg m^{-3}	Density of liquid water
σ_θ	1	Standard deviation, Cheung contact angle distribution function
σ_k	m	Standard deviation, pore type *k* in pore-size distribution
τ_k	1	Tortuosity of component *k*

REFERENCES

1. E. J. F. Dickinson, Review of Methods for Modelling the Polymer Electrolyte Membrane in the Context of a Polymer Electrolyte Membrane Fuel Cell (PEMFC), National Physical Laboratory, Teddington, UK (2019).
2. N. Djilali, *Energy*, **32**, 269 (2007).
3. E. J. F. Dickinson, Review of Methods for Modelling the Catalyst Layers of a Polymer Electrolyte Membrane Fuel Cell (PEMFC), National Physical Laboratory, Teddington, UK (2019).
4. J. H. Nam and M. Kaviany, *Int. J. Heat Mass Tran.*, **46**, 4595 (2003).
5. C. Y. Wang, *Chem. Rev.*, **104**, 4727 (2004).
6. A. Z. Weber, R. M. Darling and J. Newman, *J. Electrochem. Soc.*, **151**, A1715 (2004).
7. C. Siegel, *Energy*, **33**, 1331 (2008).
8. W. Dai, H. J. Wang, X. Z. Yuan, J. J. Martin, D. J. Yang, J. L. Qiao and J. X. Ma, *Int. J. Hydrogen Energy*, **34**, 9461 (2009).
9. K. Jiao and X. Li, *Prog. Energy Combus. Sci.*, **37**, 221 (2011).
10. N. Zamel and X. G. Li, *Prog. Energy Combus. Sci.*, **39**, 111 (2013).
11. X. L. Liu, F. Y. Peng, G. F. Lou and Z. Wen, *J. Power Sources*, **299**, 85 (2015).
12. K. W. Baek, E. S. Hong and S. W. Cha, *Int. J. Auto. Tech.*, **16**, 309 (2015).
13. C. Si, X. D. Wang, W. M. Yan and T. H. Wang, *J. Chem.* (2015).
14. M. Andersson, S. B. Beale, M. Espinoza, Z. Wu and W. Lehnertbe, *Appl. Energy*, **180**, 757 (2016).
15. E. J. F. Dickinson and G. Hinds, *J. Electrochem. Soc.*, **166**, F221 (2019).
16. M. A. Khan, B. Sundén and J. L. Yuan, *J. Power Sources*, **196**, 7899 (2011).
17. X. H. Wang and T. V. Nguyen, *J. Electrochem. Soc.*, **155**, B1085 (2008).
18. J. J. Baschuk and X. G. Li, *J. Power Sources*, **142**, 134 (2004).
19. Q. Ye and T. V. Nguyen, *J. Electrochem. Soc.*, **154**, B1242 (2007).

20. R. Banerjee and S. G. Kandlikar, *Int. J. Hydrogen Energy*, **40**, 3990 (2015).
21. S. Chang and H. Chu, *J. Power Sources*, **161**, 1161 (2006).
22. Y. Wang and K. S. Chen, *Chem. Eng. Sci.*, **66**, 3557 (2011).
23. J. Zhou, S. Shukla, A. Putz and M. Secanell, *Electrochim. Acta*, **268**, 366 (2018).
24. V. Gurau and J. A. Mann, *SIAM J. Appl. Math.*, **70**, 410 (2009).
25. I. S. Hussaini and C. Y. Wang, *J. Power Sources*, **195**, 3830 (2010).
26. P. P. Mukherjee, Q. J. Kang and C. Y. Wang, *Energy Environ. Sci.*, **4**, 346 (2011).
27. G. B. Zhang, L. H. Fan, J. Sun and K. Jiao, *Int. J. Heat Mass Tran.*, **115**, 714 (2017).
28. D. Natarajan and T. V. Nguyen, *J. Electrochem. Soc.*, **148**, A1324 (2001).
29. H. Meng, *J. Power Sources*, **171**, 738 (2007).
30. S. Strahl, A. Husar and A. A. Franco, *Int. J. Hydrogen Energy*, **39**, 9752 (2014).
31. L. Cindrella, A. M. Kannan, J. F. Lin, K. Saminathan, Y. Ho, C. W. Lin and J. Wertz, *J. Power Sources*, **194**, 146 (2009).
32. C. Quick, D. Ritzinger, W. Lehnert and C. Hartnig, *J. Power Sources*, **190**, 110 (2009).
33. Y. L. Wang, S. X. Wang, S. C. Liu, H. Li and K. Zhu, *Electrochim. Acta*, **318**, 770 (2019).
34. A. Z. Weber and M. A. Hickner, *Electrochim. Acta*, **53**, 7668 (2008).
35. X. H. Wang and T. V. Nguyen, *J. Electrochem. Soc.*, **157**, B496 (2010).
36. J. P. Owejan, J. E. Owejan, W. B. Gu, T. A. Trabold, T. W. Tighe and M. F. Mathias, *J. Electrochem. Soc.*, **157**, B1456 (2010).
37. J. M. LaManna, J. V. Bothe, F. Y. Zhang and M. M. Mench, *J. Power Sources*, **271**, 180 (2014).
38. A. El-Kharouf, T. J. Mason, D. J. L. Brett and B. G. Pollet, *J. Power Sources*, **218**, 393 (2012).
39. S. Basu, C. Y. Wang and K. S. Chen, *J. Electrochem. Soc.*, **156**, B748 (2009).
40. A. Z. Weber, R. L. Borup, R. M. Darling, P. K. Das, T. J. Dursch, W. B. Gu, D. Harvey, A. Kusoglu, S. Litster, M. M. Mench, R. Mukundan, J. P. Owejan, J. G. Pharoah, M. Secanell and I. V. Zenyuk, *J. Electrochem. Soc.*, **161**, F1254 (2014).
41. S. Kim and M. M. Mench, *J. Electrochem. Soc.*, **156**, B353 (2009).
42. F. Y. Zhang, X. G. Yang and C. Y. Wang, *J. Electrochem. Soc.*, **153**, A225 (2006).
43. S. Ge and C. Y. Wang, *J. Electrochem. Soc.*, **154**, B998 (2007).
44. I. S. Hussaini and C. Y. Wang, *J. Power Sources*, **187**, 444 (2009).
45. T. A. Trabold, J. P. Owejan, D. L. Jacobson, M. Arif and P. R. Huffman, *Int. J. Heat Mass Tran.*, **49**, 4712 (2006).
46. M. M. Mench, in *Hydrogen and Fuel Cells: Fundamentals, Technologies and Applications*, D. Stolten ed., p. 89, Wiley-VCH, Weinheim, Germany (2010).
47. S. Shimpalee, S. Greenway and J. Van Zee, *J. Power Sources*, **160**, 398 (2006).
48. X. D. Wang, Y. Y. Duan, W. M. Yan and X. F. Peng, *Electrochim. Acta*, **53**, 5334 (2008).
49. L. J. Yu, G. P. Ren, M. J. Qin and X. M. Jiang, *Renewable Energy*, **34**, 530 (2009).
50. W. M. Yan, H. S. Chu, J. Y. Chen, C. Y. Soong and F. L. Chen, *J. Power Sources*, **162**, 1147 (2006).
51. S. Shimpalee, D. Spuckler and J. Van Zee, *J. Power Sources*, **167**, 130 (2007).
52. D. M. Bernardi, *J. Electrochem. Soc.*, **137**, 3344 (1990).
53. T. F. Fuller and J. Newman, *J. Electrochem. Soc.*, **140**, 1218 (1993).
54. T. E. Springer, M. S. Wilson and S. Gottesfeld, *J. Electrochem. Soc.*, **140**, 3513 (1993).
55. A. Z. Weber and J. Newman, *Chem. Rev.*, **104**, 4679 (2004).
56. M. Wöhr, K. Bolwin, W. Schnurnberger, M. Fischer, W. Neubrand and G. Eigenberger, *Int. J. Hydrogen Energy*, **23**, 213 (1998).
57. D. M. Bernardi and M. W. Verbrugge, *AIChE J.*, **37**, 1151 (1991).
58. N. Djilali and D. Lu, *Int. J. Therm. Sci.*, **41**, 29 (2002).
59. D. Cheddie and N. Munroe, *J. Power Sources*, **147**, 72 (2005).
60. Y. Wang and C. Y. Wang, *J. Power Sources*, **147**, 148 (2005).
61. Z. X. Liu, Z. Q. Mao and C. Wang, *J. Power Sources*, **158**, 1229 (2006).
62. H. C. Liu, W. M. Yan and X. D. Wang, *J. Electrochem. Soc.*, **154**, B1338 (2007).
63. J. J. Baschuk and X. H. Li, *J. Power Sources*, **86**, 181 (2000).
64. A. Rowe and X. G. Li, *J. Power Sources*, **102**, 82 (2001).

65. D. H. Schwarz and N. Djilali, *J. Electrochem. Soc.*, **154**, B1167 (2007).
66. T. V. Nguyen and R. E. White, *J. Electrochem. Soc.*, **140**, 2178 (1993).
67. S. Dutta, S. Shimpalee and J. W. Van Zee, *J. Appl. Electrochem.*, **30**, 135 (2000).
68. P. Costamagna, *Chem. Eng. Sci.*, **56**, 323 (2001).
69. J. L. Yuan and B. Sundén, *Electrochim. Acta*, **50**, 677 (2004).
70. B. Zhou, W. B. Huang, Y. Zong and A. Sobiesiak, *J. Power Sources*, **155**, 190 (2006).
71. W.-K. Lee, S. Shimpalee and J. W. Van Zee, *J. Electrochem. Soc.*, **150**, A341 (2003).
72. M. Hossain, S. Z. Islam and P. Pollard, *Renewable Energy*, **51**, 404 (2013).
73. Y. M. Ferng, Y. C. Tzang, B. S. Pei, C. C. Sun and A. Su, *Int. J. Hydrogen Energy*, **29**, 381 (2004).
74. H. Wu, P. Berg and X. Li, *J. Power Sources*, **165**, 232 (2007).
75. J. E. Dawes, N. S. Hanspal, O. A. Family and A. Turan, *Chem. Eng. Sci.*, **64**, 2781 (2009).
76. S. R. de Groot and P. Mazur, *Non-Equilibrium Thermodynamics*, Dover Publications, Inc., New York (1984).
77. R. B. Bird, W. E. Stewart and E. N. Lightfoot, *Transport Phenomena*, John Wiley & Sons, Inc., New York (2007).
78. G. J. M. Janssen, *J. Electrochem. Soc.*, **148**, A1313 (2001).
79. A. Z. Weber and J. Newman, *J. Electrochem. Soc.*, **151**, A311 (2004).
80. A. Z. Weber and J. Newman, *J. Electrochem. Soc.*, **151**, A326 (2004).
81. L. A. Richards, *Physics*, **1**, 318 (1931).
82. D. E. Elrick, *The Physics of Fluids*, **4**, 572 (1961).
83. J. Bear, in *Modeling Phenomena of Flow and Transport in Porous Media*, J. Bear Editor, p. 367, Springer International Publishing, Cham, Switzerland (2018).
84. C. Ziegler and D. Gerteisen, *J. Power Sources*, **188**, 184 (2009).
85. M. Vynnycky, *Appl. Math. Comput.*, **189**, 1560 (2007).
86. H. K. Hsuen and K. M. Yin, *Int. J. Hydrogen Energy*, **36**, 5487 (2011).
87. K. Promislow, J. Stockie and B. Wetton, *Proc. Roy. Soc. A*, **462**, 789 (2006).
88. M. Vynnycky and A. Gordon, *Proc. Roy. Soc. A*, **469** (2013).
89. K. M. Yin and H. K. Hsuen, *Fuel Cells*, **13**, 1213 (2013).
90. G. B. Zhang and K. Jiao, *J. Power Sources*, **391**, 120 (2018).
91. H. Meng, *Int. J. Hydrogen Energy*, **34**, 5488 (2009).
92. V. Gurau, R. V. Edwards, J. A. Mann and T. A. Zawodzinski, *Electrochem. Solid State Lett.*, **11**, B132 (2008).
93. D. Natarajan and T. V. Nguyen, *J. Power Sources*, **115**, 66 (2003).
94. L. Matamoros and D. Bruggemann, *J. Power Sources*, **161**, 203 (2006).
95. C. Ziegler, H. Yu and J. Schumacher, *J. Electrochem. Soc.*, **152**, A1555 (2005).
96. P. Rama, R. Chen and R. Thring, *Proc. IMechE A J. Power and Energy*, **220**, 535 (2006).
97. P. Rama and R. Chen, *J. Fuel Cell Sci. Tech.*, **7** (2010).
98. D. T. Song, Q. P. Wang, Z. S. Liu and C. Huang, *J. Power Sources*, **159**, 928 (2006).
99. N. Akhtar and P. Kerkhof, *Int. J. Hydrogen Energy*, **36**, 5536 (2011).
100. L. B. Wang, N. I. Wakayama and T. Okada, *Electrochem. Commun.*, **4**, 584 (2002).
101. E. Birgersson, M. Noponen and M. Vynnycky, *J. Electrochem. Soc.*, **152**, A1021 (2005).
102. M. Acosta, C. Merten, G. Eigenberger, H. Class, R. Helmig, B. Thoben and H. Muller-Steinhagen, *J. Power Sources*, **159**, 1123 (2006).
103. A. A. Shah, G. S. Kim, P. C. Sui and D. Harvey, *J. Power Sources*, **163**, 793 (2007).
104. J. J. Hwang, *J. Power Sources*, **164**, 174 (2007).
105. C. J. Bapat and S. T. Thynell, *J. Power Sources*, **179**, 240 (2008).
106. K. Jiao and X. G. Li, *Electrochim. Acta*, **54**, 6876 (2009).
107. D. S. Chan and K. L. Hsueh, *Energies*, **3**, 920 (2010).
108. A. C. Olesen, T. Berning and S. K. Kær, *J. Fuel Cell Sci. Tech.*, **9** (2012).
109. D. Fofana, J. Hamelin and P. Benard, *Int. J. Hydrogen Energy*, **38**, 10050 (2013).
110. M. Abdollahzadeh, P. Ribeirinha, M. Boaventura and A. Mendes, *Energy*, **152**, 939 (2018).
111. L. Xing, W. D. Shi, P. K. Das and K. Scott, *AIChE J.*, **63**, 4895 (2017).
112. P. Havaej, M. J. Kermani, M. Abdollahzadeh, H. Heidary and A. Moradi, *Int. J. Hydrogen Energy*, **43**, 10031 (2018).

113. Z. Penga, C. Bergbreiter, F. Barbir and J. Scholta, *Energy Convers. Manag.*, **189**, 167 (2019).
114. O. B. Rizvandi and S. Yesilyurt, *Electrochim. Acta*, **302**, 180 (2019).
115. C. Y. Wang, *Electrochem. Solid State Lett.*, **12**, S2 (2009).
116. S. Whitaker, *AIChE J.*, **13**, 420 (1967).
117. C. Y. Wang and P. Cheng, *Int. J. Heat Mass Tran.*, **39**, 3607 (1996).
118. C. Y. Wang and P. Cheng, in *Advances in Heat Transfer*, J. P. Hartnett, J. T. F. Irvine, Y. I. Cho and G. A. Greene eds., p. 93, Elsevier (1997).
119. Z. H. Wang, C. Y. Wang and K. S. Chen, *J. Power Sources*, **94**, 40 (2001).
120. U. Pasaogullari and C. Y. Wang, *J. Electrochem. Soc.*, **152**, A380 (2005).
121. S. Mazumder and J. V. Cole, *J. Electrochem. Soc.*, **150**, A1510 (2003).
122. L. M. Abriola and G. F. Pinder, *Water Resour. Res.*, **21**, 11 (1985).
123. C.-Y. Wang and C. Beckermann, *Int. J. Heat Mass Tran.*, **36**, 2747 (1993).
124. M. R. Hu, A. Z. Gu, M. H. Wang, X. J. Zhu and L. J. Yu, *Energy Convers. Manag.*, **45**, 1861 (2004).
125. U. Pasaogullari and C. Y. Wang, *Electrochim. Acta*, **49**, 4359 (2004).
126. Y. Wang and C.-Y. Wang, *J. Electrochem. Soc.*, **153**, A1193 (2006).
127. U. Pasaogullari, P. P. Mukherjee, C. Y. Wang and K. S. Chen, *J. Electrochem. Soc.*, **154**, B823 (2007).
128. H. Ju, *J. Power Sources*, **191**, 259 (2009).
129. J. Nam, P. Chippar, W. Kim and H. Ju, *Appl. Energy*, **87**, 3699 (2010).
130. P. Chippar, O. Kyeongmin, K. Kang and H. Ju, *Int. J. Hydrogen Energy*, **37**, 6326 (2012).
131. L. Hao, K. Moriyama, W. B. Gu and C. Y. Wang, *J. Electrochem. Soc.*, **163**, F744 (2016).
132. A. Jo, G. Gwak, M. Moazzam, J. Lee and H. Ju, *Int. J. Hydrogen Energy*, **42**, 3731 (2017).
133. V. Gurau, *Electrochem. Solid State Lett.*, **12**, S4 (2009).
134. P. K. Das, X. G. Li, Z. Xie and Z. S. Liu, *Int. J. Energy Res.*, **35**, 1325 (2011).
135. A. A. Kulikovsky, *J. Electrochem. Soc.*, **150**, A1432 (2003).
136. C. Z. Qin and S. M. Hassanizadeh, *Int. J. Heat Mass Tran.*, **70**, 693 (2014).
137. M. Coppo, N. P. Siegel and M. R. von Spakovsky, *J. Power Sources*, **159**, 560 (2006).
138. C. Z. Qin and S. M. Hassanizadeh, *Int. J. Hydrogen Energy*, **40**, 3348 (2015).
139. A. Z. Weber, *J. Power Sources*, **195**, 5292 (2010).
140. M. C. Leverett, *AIME Trans.*, **142**, 152 (1941).
141. T. Berning, M. Odgaard and S. K. Kaer, *J. Electrochem. Soc.*, **156**, B1301 (2009).
142. Z. Y. Shi, X. Wang and L. Guessous, *J. Fuel Cell Sci. Tech.*, **7** (2010).
143. K. S. Udell, *Int. J. Heat Mass Tran.*, **28**, 485 (1985).
144. U. Pasaogullari and C. Y. Wang, *J. Electrochem. Soc.*, **151**, A399 (2004).
145. D. S. Falcão, P. J. Gomes, V. B. Oliveira, C. Pinho and A. M. F. R. Pinto, *Int. J. Hydrogen Energy*, **36**, 12486 (2011).
146. E. C. Kumbur, K. V. Sharp and M. M. Mench, *J. Power Sources*, **168**, 356 (2007).
147. D. Gerteisen, T. Heilmann and C. Ziegler, *J. Power Sources*, **187**, 165 (2009).
148. T. Berning, M. Odgaard and S. K. Kraer, *J. Power Sources*, **196**, 6305 (2011).
149. S. Balasubramanian and A. Z. Weber, in *Physical Multiscale Modeling and Numerical Simulation of Electrochem. Devices for Energy Conversion and Storage: From Theory to Engineering to Practice*, A. A. Franco, M. L. Doublet and W. G. Bessler eds., p. 91, Springer-Verlag, London (2016).
150. J. T. Gostick, M. W. Fowler, M. A. Ioannidis, M. D. Pritzker, Y. M. Volfkovich and A. Sakars, *J. Power Sources*, **156**, 375 (2006).
151. E. C. Kumbur, K. V. Sharp and M. M. Mench, *J. Electrochem. Soc.*, **154**, B1315 (2007).
152. E. C. Kumbur, K. V. Sharp and M. M. Mench, *J. Electrochem. Soc.*, **154**, B1305 (2007).
153. V. P. Schulz, J. Becker, A. Wiegmann, P. P. Mukherjee and C. Y. Wang, *J. Electrochem. Soc.*, **154**, B419 (2007).
154. K. Steinkamp, J. O. Schumacher, F. Goldsmith, M. Ohlberger and C. Ziegler, *J. Fuel Cell Sci. Tech.*, **5** (2008).
155. N. Zamel and X. G. Li, *Int. J. Energy Res.*, **32**, 698 (2008).
156. V. Gurau and J. A. Mann, *J. Electrochem. Soc.*, **157**, B512 (2010).
157. T. V. Nguyen, *J. Electrochem. Soc.*, **143**, L103 (1996).

158. X. Ye and C. Wang, *J. Electrochem. Soc.*, **154**, B676 (2007).
159. V. Mulone and K. Karan, *Int. J. Hydrogen Energy*, **38**, 558 (2013).
160. V. Gurau, T. A. Zawodzinski and J. A. Mann, *J. Fuel Cell Sci. Tech.*, **5** (2008).
161. T. Koido, T. Furusawa and K. Moriyama, *J. Power Sources*, **175**, 127 (2008).
162. J. T. Gostick, M. A. Ioannidis, M. W. Fowler and M. D. Pritzker, *J. Power Sources*, **194**, 433 (2009).
163. P. O. Olapade, J. P. Meyers, R. Mukundan, J. R. Davey and R. L. Borup, *J. Electrochem. Soc.*, **158**, B536 (2011).
164. X. D. Wang, Y. L. Wang, Y. Chen, C. Si, A. Su and D. J. Lee, *J. Taiwan Inst. Chem. Eng.*, **45**, 1532 (2014).
165. B. Ramos-Alvarado, A. Hernandez-Guerrero and M. W. Ellis, *J. Power Sources*, **232**, 376 (2013).
166. S. M. Senn and D. Poulikakos, *J. Heat Trans.*, **127**, 1245 (2005).
167. E. C. Kumbur, K. V. Sharp and M. M. Mench, *J. Electrochem. Soc.*, **154**, B1295 (2007).
168. T. V. Nguyen, G. Y. Lin, H. B. Ohn, D. Hussey, D. Jacobson and M. Arif, *ECS Trans.*, **3**, 415 (2006).
169. T. V. Nguyen, G. Lin, H. Ohn and X. Wang, *Electrochem. Solid State Lett.*, **11**, B127 (2008).
170. J. T. Gostick, M. A. Ioannidis, M. W. Fowler and M. D. Pritzker, *Electrochem. Commun.*, **10**, 1520 (2008).
171. Y. M. Volfkovich, V. S. Bagotzky, V. E. Sosenkin and I. A. Blinov, *Colloid. Surface A*, **187**, 349 (2001).
172. J. D. Fairweather, P. Cheung, J. St-Pierre and D. T. Schwartz, *Electrochem. Commun.*, **9**, 2340 (2007).
173. K. G. Gallagher, R. M. Darling, T. W. Patterson and M. L. Perry, *J. Electrochem. Soc.*, **155**, B1225 (2008).
174. P. Cheung, J. D. Fairweather and D. T. Schwartz, *J. Power Sources*, **187**, 487 (2009).
175. P. Ustohal, F. Stauffer and T. Dracos, *J. Contam. Hydrol.*, **33**, 5 (1998).
176. S. Dwenger, G. Eigenberger and U. Nieken, *Transport Porous Med.*, **91**, 281 (2012).
177. A. Kusoglu, A. Kwong, K. T. Clark, H. P. Gunterman and A. Z. Weber, *J. Electrochem. Soc.*, **159**, F530 (2012).
178. J. Zhou, A. Putz and M. Secanell, *J. Electrochem. Soc.*, **164**, F530 (2017).
179. E. Nishiyama and T. Murahashi, *J. Power Sources*, **196**, 1847 (2011).
180. J. H. Chun, K. T. Park, D. H. Jo, S. G. Kim and S. H. Kim, *Int. J. Hydrogen Energy*, **36**, 1837 (2011).
181. D. L. Wood, C. Rulison and R. L. Borup, *J. Electrochem. Soc.*, **157**, B195 (2010).
182. T. Rosén, J. Eller, J. Kang, N. I. Prasianakis, J. Mantzaras and F. N. Büchi, *J. Electrochem. Soc.*, **159**, F536 (2012).
183. H. Ju, G. Luo and C. Y. Wang, *J. Electrochem. Soc.*, **154**, B218 (2007).
184. A. T. Corey, *Producers Monthly*, **19**, 38 (1954).
185. L. Fan, G. Zhang and K. Jiao, *Energy Convers. Manag.*, **150**, 763 (2017).
186. J. T. Gostick, M. W. Fowler, M. D. Pritzker, M. A. Ioannidis and L. M. Behra, *J. Power Sources*, **162**, 228 (2006).
187. N. T. Burdine, *J. Petrol. Tech.*, **5**, 71 (1953).
188. Y. Mualem, *Water Resour. Res.*, **12**, 513 (1976).
189. H. Meng and C. Y. Wang, *J. Electrochem. Soc.*, **152**, A1733 (2005).
190. I. V. Zenyuk, P. K. Das and A. Z. Weber, *J. Electrochem. Soc.*, **163**, F691 (2016).
191. M. S. Ismail, D. B. Ingham, K. J. Hughes, L. Ma and M. Pourkashanian, *Int. J. Hydrogen Energy*, **40**, 10994 (2015).
192. A. Iranzo, M. Munoz, F. Rosa and J. Pino, *Int. J. Hydrogen Energy*, **35**, 11533 (2010).
193. G. Y. Lin, W. S. He and T. V. Nguyen, *J. Electrochem. Soc.*, **151**, A1999 (2004).
194. J. P. Owejan, T. A. Trabold and M. M. Mench, *Int. J. Heat Mass Tran.*, **71**, 585 (2014).
195. P. K. Das, X. G. Li and Z. S. Liu, *Appl. Energy*, **87**, 2785 (2010).
196. Y. L. Wang and S. X. Wang, *Int. J. Heat Mass Tran.*, **105**, 18 (2017).
197. P. A. García-Salaberri, J. T. Gostick, G. Hwang, A. Z. Weber and M. Vera, *J. Power Sources*, **296**, 440 (2015).

198. P. A. García-Salaberri, G. Hwang, M. Vera, A. Z. Weber and J. T. Gostick, *Int. J. Heat Mass Tran.*, **86**, 319 (2015).
199. M. M. Tomadakis and S. V. Sotirchos, *AIChE J.*, **39**, 397 (1993).
200. A. Jayakumar, S. P. Sethu, M. Ramos, J. Robertson and A. Al-Jumaily, *Ionics*, **21**, 1 (2015).
201. R. Wu, Q. Liao, X. Zhu and H. Wang, *Int. J. Heat Mass Tran.*, **54**, 4341 (2011).
202. M. Eikerling and A. Kornyshev, *J. Electroanal. Chem.*, **453**, 89 (1998).
203. D. M. Bernardi and M. W. Verbrugge, *J. Electrochem. Soc.*, **139**, 2477 (1992).
204. C. Y. Wang, W. B. Gu and B. Y. Liaw, *J. Electrochem. Soc.*, **145**, 3407 (1998).
205. H. Meng, *J. Power Sources*, **168**, 218 (2007).
206. K. M. Yin, H. K. Hsuen, Y. A. Kung and B. S. Cheng, *J. Taiwan Inst. Chem. Eng.*, **63**, 133 (2016).
207. W. S. He, J. S. Yi and T. V. Nguyen, *AIChE J.*, **46**, 2053 (2000).
208. K. M. Yin, H. K. Hsuen and Y. A. Kung, *J. Taiwan Inst. Chem. Eng.*, **45**, 2358 (2014).
209. A. A. Shah, G. S. Kim, W. Gervais, A. Young, K. Promislow, J. Li and S. Ye, *J. Power Sources*, **160**, 1251 (2006).
210. T. Berning, M. Odgaard and S. K. Kaer, *J. Power Sources*, **195**, 4842 (2010).
211. R. J. Balliet and J. Newman, *J. Electrochem. Soc.*, **158**, B927 (2011).
212. B. Abramzon and W. A. Sirignano, *Int. J. Heat Mass Tran.*, **32**, 1605 (1989).
213. C. Fink and N. Fouquet, *Electrochim. Acta*, **56**, 10820 (2011).
214. A. Z. Weber and J. Newman, *J. Electrochem. Soc.*, **152**, A677 (2005).
215. K. Kang and H. Ju, *J. Power Sources*, **194**, 763 (2009).
216. J. S. Preston, R. S. Fu, U. Pasaogullari, D. S. Hussey and D. L. Jacobson, *J. Electrochem. Soc.*, **158**, B239 (2011).
217. G. H. Song and H. Meng, *Acta Mech. Sinica*, **29**, 318 (2013).
218. R. Anderson, L. Zhang, Y. Ding, M. Blanco, X. Bi and D. Wilkinson, *J. Power Sources*, **195**, 4531 (2010).
219. H. Wu, X. G. Li and P. Berg, *Electrochim. Acta*, **54**, 6913 (2009).
220. G. B. Zhang, X. Xie, B. A. Xie, Q. Du and K. Jiao, *Int. J. Heat Mass Tran.*, **130**, 555 (2019).
221. T. Berning and N. Djilali, *J. Electrochem. Soc.*, **150**, A1589 (2003).
222. M. A. R. Sadiq Al-Baghdadi and H. A. K. Shahad Al-Janabi, *Energy Convers. Manag.*, **48**, 3102 (2007).
223. M. Abdollahzadeh, J. C. Pascoa, A. A. Ranjbar and Q. Esmaili, *Energy*, **68**, 478 (2014).
224. G. L. He, P. W. Ming, Z. C. Zhao, A. Abudula and Y. Xiao, *J. Power Sources*, **163**, 864 (2007).
225. G. L. He, Y. Yamazaki and A. Abudula, *J. Power Sources*, **194**, 190 (2009).
226. M. Ishii and N. Zuber, *AIChE J.*, **25**, 843 (1979).
227. G. B. Zhang and K. Jiao, *Energy Convers. Manag.*, **176**, 409 (2018).
228. X. L. Liu, G. F. Lou and Z. Wen, *J. Power Sources*, **195**, 2764 (2010).
229. N. Khajeh-Hosseini-Dalasm, K. Fushinobu and K. Okazaki, *Int. J. Hydrogen Energy*, **35**, 4234 (2010).
230. T. F. Cao, H. Lin, L. Chen, Y. L. He and W. Q. Tao, *Appl. Energy*, **112**, 1115 (2013).
231. A. Jarauta and P. Ryzhakov, *Arch. Comput. Methods Eng.*, **25**, 1027 (2018).
232. L. Chen, T. F. Cao, Z. H. Li, Y. L. He and W. Q. Tao, *Int. J. Hydrogen Energy*, **37**, 9155 (2012).
233. W. M. Yan, H. Y. Li and W. C. Tsai, *J. Electrochem. Soc.*, **153**, A1984 (2006).
234. Y. Wang, S. Basu and C. Y. Wang, *J. Power Sources*, **179**, 603 (2008).
235. C. Z. Qin, D. Rensink, S. Fell and S. M. Hassanizadeh, *J. Power Sources*, **197**, 136 (2012).
236. R. Anderson, L. F. Zhang, Y. L. Ding, M. Blanco, X. T. Bi and D. P. Wilkinson, *J. Power Sources*, **195**, 4531 (2010).
237. S. Basu, J. Li and C. Y. Wang, *J. Power Sources*, **187**, 431 (2009).
238. H. M. Yu, C. Ziegler, M. Oszcipok, M. Zobel and C. Hebling, *Electrochim. Acta*, **51**, 1199 (2006).
239. T. Soboleva, K. Malek, Z. Xie, T. Navessin and S. Holdcroft, *ACS Appl. Mater. Interf.*, **3**, 1827 (2011).

240. B. Andreaus and M. Eikerling, in *Device and Materials Modeling in PEM Fuel Cells*, S. J. Paddison and K. S. Promislow eds., p. 41, Springer-Verlag, New York (2009).
241. M. Eikerling, *J. Electrochem. Soc.*, **153**, E58 (2006).
242. N. P. Siegel, M. W. Ellis, D. J. Nelson and M. R. von Spakovsky, *J. Power Sources*, **128**, 173 (2004).
243. C. Y. Jung and S. C. Yi, *Electrochem. Commun.*, **35**, 34 (2013).
244. T. Suzuki, K. Kudo and Y. Morimoto, *J. Power Sources*, **222**, 379 (2013).
245. H. Wu, P. Berg and X. G. Li, *Appl. Energy*, **87**, 2778 (2010).
246. X. Zhang, D. T. Song, Q. P. Wang, C. Huang, Z. S. Liu and A. A. Shah, *J. Fuel Cell Sci. Tech.*, **7** (2010).
247. W. C. Sheng, H. A. Gasteiger and Y. Shao-Horn, *J. Electrochem. Soc.*, **157**, B1529 (2010).
248. C. Marr and X. G. Li, *J. Power Sources*, **77**, 17 (1999).
249. N. Khajeh-Hosseini-Dalasm, M. J. Kermani, D. G. Moghaddam and J. M. Stockie, *Int. J. Hydrogen Energy*, **35**, 2417 (2010).
250. R. M. Rao, D. Bhattacharyya, R. Rengaswamy and S. R. Choudhury, *J. Power Sources*, **173**, 375 (2007).
251. L. Xing, S. F. Du, R. Chen, M. Mamlouk and K. Scott, *Energy*, **96**, 80 (2016).
252. L. Xing, M. Mamlouk, R. Kumar and K. Scott, *Int. J. Hydrogen Energy*, **39**, 9087 (2014).
253. S. A. Li, J. L. Yuan, G. B. Xie and B. Sundén, *Int. J. Hydrogen Energy*, **43**, 8451 (2018).
254. G. A. Futter, P. Gazdzicki, A. Friedrich, A. Latz and T. Jahnke, *J. Power Sources*, **391**, 148 (2018).
255. T. Swamy, E. C. Kumbur and M. M. Mench, *J. Electrochem. Soc.*, **157**, B77 (2010).
256. A. R. Kalidindi, R. Taspinar, S. Litster and E. C. Kumbur, *Int. J. Hydrogen Energy*, **38**, 9297 (2013).